NTNU
Norwegian University of
Science and Technology

Development of polymer-nanoparticle composite with high refractive index

Ola Gjønnes Grendal

Materials Science and Engineering
Submission date: June 2016
Supervisor: Mari-Ann Einarsrud, IMTE
Co-supervisor: Antoine Dalod, IMTE

Norwegian University of Science and Technology
Department of Materials Science and Engineering

Declaration

I hereby declare that the work presented in this document has been performed independently and in accordance with the rules and regulations of the NTNU Norwegian University of Science and Technology.

Trondheim, June 13, 2016

Ola Gjønnes Grendal

Preface

This thesis is submitted to NTNU Norwegian University of Science and Technology as a part of the requirements for the degree of Master of Science. The work leading up to this thesis have been conducted at the Department of Materials Science and Engineering at NTNU between January 18 and June 13, 2016. Professor Mari-Ann Einarsrud have supervised the work while Ph.D. candidate Antoine Robert Marie Dalod has been co-supervisor.

I would like to thank both Mari-Ann Einarsrud and Antoine Robert Marie Dalod for valuable guidance through this work, both helping with feedback and insightful discussions. Antoine Robert Marie Dalod has also been very helpful and supportive in the day-to-day work, giving valuable tips and support when needed.

Staff Engineer Vedran Furtula and Postdoc Eric Karhu, both at Department of Physics, is acknowledge for giving access to, and helping with performing measurements of refractive index and transmittance respectively. I would also like to thank the technical staff at the department and at NTNU NanoLab for giving equipment training and support when needed. poLight AS is acknowledge for supplying me with their polymer named P53.

Finally, I would like to thank my fellow student Kent Mogstad, and my friends Jens Nikolai Berdal Kortner and Morten Andreas Løchen for helping me proofread the final draft.

Abstract

A newly developed lens technology utilizes a soft high refractive index polymer to change focus. By further increasing the refractive index of the polymer, without lowering the transmittance of visible light, the overall lens properties will be improved. Dispersion of TiO_2 nanoparticles into the polymer was chosen for this because of TiO_2 high refractive index.

In this work, a polymer-nanoparticle composite with high refractive index is developed by dispersing TiO_2 nanoparticles into the polymer. The polymer-nanoparticle composite was characterized with respect to refractive index and transmittance of visible light. A major part of the work evolved around achieving a homogenous dispersion of non-agglomerated TiO_2 nanoparticles. Different approaches was used, including *in situ* functionalization and *post* synthesis methods like ultrasonification and electrostatic stabilization of the TiO_2 nanoparticles. Non of the approaches were successful in achieving non-agglomerated particles, making the polymer-nanoparticle composite milky white, and the transmittance of visible light very low. A small increase in refractive index was observed. This approach for making a polymer-nanoparticle composite with high refractive index and high transmittance of visible light is promising, but further work on achieving non-agglomerated particles must be done.

The TiO_2 nanoparticles used were made by a hydrothermal synthesis route with titanium (IV) isopropoxied (TIP) as precursor, and *in situ* functionalized with 3-aminopropyl trietoxhysilane (APTES). The effect of different synthesis parameters (shorter reaction time, lower reaction temperature and acidic *versus* basic reaction conditions) on the size and morphology of the synthesized particles were investigated. A drastic change in morphology was observed between acidic and basic reaction conditions. Under basic reaction conditions, big elongated particles (up to 200 nm long) formed, while for acidic reaction conditions only small spherical particles (around 10 nm) were observed. This was believed to arise from a combination of oriented attachment and specific adsorption of APTES to different crystallographic faces.

Sammendrag

En nylig utviklet linse utnytter en myk polymer med høy brytningsindeks for å endre fokus. Ved å øke brytningsindeksen til polymeren, uten å senke transmisjon av synlig lys gjennom den, vil de optiske egenskapene til linsen forbedres. Ved å dispergere TiO_2 nanopartikler i polymeren kan brytningsindeksen til polymeren økes på grunn av den høye brytningsindeksen til TiO_2.

I dette arbeidet blir en polymer-nanopartikkel kompositt med høy brytningsindeks utviklet ved å dispergere TiO_2 nanopartikler inn i polymeren. Polymer-nanopartikel kompositten blir karakterisert med hensyn til brytningsindeks og transmisjon av synlig lys. En stor del av arbeidet gikk ut på å lage en stabil dispersjon av ikke-agglomererte TiO_2 nanopartikler. Flere tilnærminger ble brukt, inkludert *in situ* funksjonalisering og *post* syntese metoder som ultralyd og elektrostatisk stabilisering av TiO_2 nanopartiklene. Ingen av metodene var vellykkede i å framstille stabile dispersjoner av ikke-agglomererte partikler, noe som førte til at polymer-nanopartikkel kompositten fikk en melkehvit farge, og hadde en veldig lav transmisjon av synlig lys. En liten økning i bytningsindeks ble observert. Denne metoden for å framstille en polymer-nanopartikkel kompositt med høy brytningsindeks og transmisjon av synlig lys virker lovende, men noe mer arbeid må gjøres for å oppnå ikke-agglomererte partikler.

TiO_2 nanopartiklene som ble brukt var laget med hydrotermisk syntese fra en titan (IV) isopropoksid (TIP) forløper, og *in situ* funksjonalisert med 3-aminopropyl triethoxsilan (APTES). Effekten av forskjellige syntese parametere (kortere reaksjonstid, lavere reaksjonstemperatur og basisk *versus* surt reaksjonsmiljø) ble undersøkt på nanopartiklenes størrelse og morfologi. En drastisk endring i morfologi ble observert ved å sammenligne basisk og surt reaksjonsmiljø. Basisk reaksjonsmiljø ga store avlange partikler (lengde opp til 200 nm), mens surt reaksjonsmiljø ga små runde partikler (10 nm i diamter). Dette ble forklart med en kombinasjon av orientert kobling av nanopartikler og spesifikk adsorpsjon av APTES på krystallografiske sider.

Contents

List of Figures

List of Tables

Chapter 1

Background

1.1 Motivation

TLens® is the name of a lens newly developed by poLight AS[1], a company located in Horten, Norway. Due to the small dimensions (3.2mm x 3.2mm x 0.4mm) of the lens its applications are mainly in cellphones and similar small electronic devices, and in March 2015 poLight AS and cellphone manufacturer BARTEC PIXAVI AS[2] announced that TLens® will be incorporated into BARTEC PIXAVI AS cellphones [1].

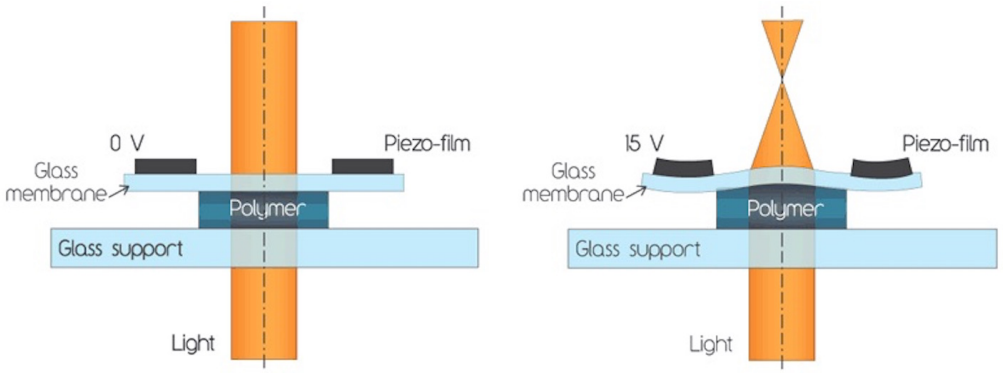

Figure 1.1: Schematic of the newly developed TLens® showing changing focus. Retrieved from ref [2].

In contrast to the lenses which are normally used in cellphones today, the TLens® consists of no moving parts for changing focus, but a soft polymer sandwiched between a glass support and a thin glass membrane. To change

[1]poLight AS homepage: `http://www.polight.no/`
[2]BARTEC PIXAVI AS homepage: `https://www.pixavi.com/`

Table 1.1: Comparison of refractive index, density and abundance between TiO_2 and featured oxides. Note, refractive index and density is dependent on the polymorph.

	Properties		
Material	Refractive index, n [-]	Density, ρ [g cm^{-3}]	Cations abundance in earth's crust by mass[1] [%]
TiO_2 (anatase)	2.5	3.8	0.7
Al_2O_3	1.8	4.0	8
ZrO_2	2.1	5.9	0.01
CuO	2.6	6.4	0.007
SiO_2	1.5	2.6	27

the focus of this lens, the glass membrane and the polymer are deformed by piezoelectric actuators placed on the glass membrane, as shown in Figure 1.1. This design makes it the smallest autofocus lens on the market, in addition to being faster and more energy efficient than its contenders [2].

An ongoing collaboration between poLight AS, University College of Southeast Norway and NTNU Norwegian University of Science and Technology is working on further improving this technology through the project *Beat the human eye*. One of the goals of the project is to increase the refractive index (n) of the polymer, since this will increase the optical power (P) of the lens ($P \propto n$). The increase in refractive index must be achieved without impairing two key features of the lens, which is high transmittance of visible light, and low stiffness. This increase in refractive index can be achieved by dispersing nanoparticles of a material with high refractive index into the polymer matrix, as done in the work from Rizhaupt-Kleissl *et al.* [3]. Such materials are often inorganic materials, and Table 1.1 presents a comparison of some featured oxides with respect to refractive index, density and abundance in earths crust. For this work, TiO_2 is chosen because of its relatively low density (which makes it disperse more easily) and high refractive index (needs to be higher than the refractive index of the polymer used in the lens, which is 1.53).

A big challenge with this method is to overcome nanoparticles tendency to agglomerate. For all materials, the ultimate goal is to lower its Gibbs free energy. Knowing that all surfaces have an increased Gibbs free energy compared with the bulk, because of unsaturated or dangling bonds, it is clear that particles want to cluster together to lower the specific surface

[1] Values retrieved from `http://periodictable.com/Properties/A/CrustAbundance.v.html`. Last visited 12.05.2016.

area (area divided by mass [m^2g^{-1}]). For nanoparticles, which have a high specific surface area, the driving force for agglomeration is high, and can be overcome by the use of surfactants [4] or electrostatic stabilization [5]. In addition, the high interface energy between inorganic and organic materials gives an additional driving force for agglomeration in this application. This can be suppressed by functionalization of the nanoparticles surface with a grafting agent [6].

1.2 Aim of the work

The main goal of this Master's thesis is to increase the refractive index of the polymer used in poLights AS TLens® by dispersing TiO_2 nanoparticles into the polymer matrix. Different approaches will be used to achieve a homogenous dispersion of non-agglomerated particles in the polymer, including *in situ* functionalization and *post* synthesis methods like ultrasonification, electrostatic stabilization and surfactants. The effect of different amounts of nanoparticles will be investigated. The polymer-nanoparticle composites will be characterized with respect to optical and mechanical properties,, by use of ellipsometer, ultraviolet-visible (UV-vis) spectroscopy and nanomechanical testing by atomic force microscope (AFM).

The TiO_2 nanoparticles used in this work are synthesized with a hydrothermal synthesis route that *in situ* functionalizes the particles, which was proposed by Dalod *et al.* [7]. This synthesis route was further optimized and investigated in the author's specialization project [8]. In this work a further investigation and optimization of the synthesis route is done. Here the effect of lower reaction temperature and acidic and basic reaction media is investigated. The synthesized particles will be characterized with respect to particle size and surface area, crystallite size, phase composition, morphology, grafting efficiency and degree of agglomeration. Methods will include X-ray diffraction (XRD), scanning electron microscope (SEM), thermogravimetric analysis (TGA) and N_2 adsorption. Further, Fourier transformed infrared spectroscopy (FTIR) will be used on the particles synthesized as a part of this work and the author's specialization project, for investigation of the bonds forming between the particle surface and grafting agent.

Chapter 2

Introduction

2.1 Optics

2.1.1 Lenses

A bi-convex lens that converges light rays to a single point, called the focal point or focus point of the lens, alongside a bi-concave lens that diverges light, is illustrated in Figure 2.1. The focal point for the diverging lens is defined as the point where the diverging light rays seem to radiate from. The length from the lens to the focal point along the optical axis (horisontal dashed line in Figure 2.1) is called the focal length (f). The focal length of a lens in air can be calculated with the lens maker's equation, shown in Equation 2.1.

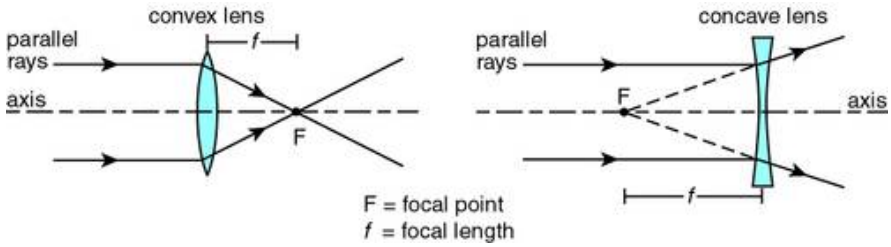

Figure 2.1: Schematic of how a bi-convex (left) and bi-concave (right) lens converges and diverges light respectively. Focal point (F) and focal length (f) are also indicated.[1]

$$\frac{1}{f} = (n-1)(\frac{1}{R_1} - \frac{1}{R_2} + \frac{(n-1)d}{nR_1R_2}) \tag{2.1}$$

[1]This picture is reused under the Creative Commons Attribution Share-Alike 2.5 License.

Here n is the refractive index of the lens material, R_1 and R_2 are the radii of curvature of the two sides of the lens, and d is the thickness of the lens at the optical axis. For a plano-convex lens, where one of the sides is flat (i.e. $R = \infty$), Equation 2.1 simplifies to Equation 2.2. A plano-convex lens is representative for TLens®. Here the sign indicates the direction of illumination, i.e. if the lens diverges or converges light.

$$\frac{1}{f} = \pm(n-1)(\frac{1}{R}) \tag{2.2}$$

Optical power (P), also called focusing power, is a measure of how strongly a lens bends light, and it is defined as the inverse of the focal length, as shown in Equation 2.3.

$$P = \frac{1}{f} \tag{2.3}$$

From Equation 2.2 and 2.3 it is clear that an increase in optical power can be achieved by increasing the refractive index of the lens material, decreasing the radii of curvature, or a combination of these two. For conventional lenses made of glass or a hard polymer, neither of these options are possible to change after fabrication of the lens. To be able to change focus, i.e. change optical power, multiple lenses are used, and moved relative to each other. One of the key features of the new TLens® is its ability to change radii of curvature after fabrication, but this change is limited. By increasing the refractive index of the polymer, small changes in radii of curvature gives a greater change in optical power, improving the overall optical power of the lens. This increase in refractive index have been shown to be possible by dispersing particles with a high refractive index into the polymer matrix [3].

2.1.2 Scattering of light

Particles dispersed in a transparent matrix will scatter light [9], as illustrated in Figure 2.2, and thus lower the transmittance of light through the matrix. For lenses, high transmittance of visible light is of utmost importance to achieve high quality pictures. For particles having the same size as the wavelength of light, the scattering power is described by Rayleigh scattering, and the mathematical formula is given in Equation 2.4.

$$P_{\text{Scat}} = 24\pi^4 P_0 \rho \frac{n_{\text{p}} - n_{\text{m}}}{n_{\text{m}}^2} \frac{V^2}{\lambda^4} \tag{2.4}$$

Here P_0 is the incident power, ρ is the concentration of particles, n_{p} and n_{m} is the refractive index of the particles and matrix respectively, V is

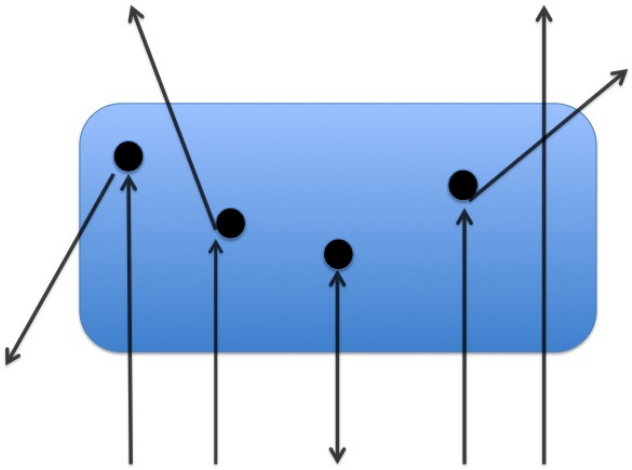

Figure 2.2: Schematic of light being scattered on its way through a matrix with dispersed particles, and thus lowering the transmittance of light through the matrix.

the volume of a single particle and λ is the wavelength of light. Assuming Rayleigh scattering and randomly dispersed particles, the transmittance (T) can then be described as shown in Equation 2.5 [10].

$$T = \frac{I}{I_0} = \exp\left\{-\frac{32\pi^4\phi_\mathrm{p}xr^3n_\mathrm{m}^4}{\lambda^4}\left(\frac{(n_\mathrm{p}/n_\mathrm{m})^2-1}{(n_\mathrm{p}/n_\mathrm{m})^2+2}\right)^2\right\} \tag{2.5}$$

I and I_0 are the intensities for transmitted and incident light respectively, ϕ_p is the volum fraction of particles, r is the particle radius, x is optical path length and the rest is as described for Equation 2.4. From Equation 2.4 and 2.5 there are mainly two ways of suppressing scattering, and therefore increasing the transmittance, and that is to decrease the particle size, or match the refractive index of particles and matrix. Matching the refractive indexes (n_p=n_m) will lead to equal intensity for incident and transmitted light, i. e. high transmittance. This will on the other hand not give an increase in refractive index for the combined system of particles and matrix, as seen from Equation 2.6 [11].

$$n_\mathrm{Composite} = n_\mathrm{p}\phi_\mathrm{p} + n_\mathrm{m}\phi_\mathrm{m} \tag{2.6}$$

Here n and ϕ represents refractive index and volum fractions respectively. Dispersing particles with a particle size smaller than the wavelength of visible

light will therefore be the way to go for achieving a higher refractive index while still keeping a high transmittance of light through the polymer for use in poLight AS TLens®. This is also shown in the work by Li *et al.* [12]. They investigated the effect of different sized alumina particles had on the transmittance through a gelatin film, and Figure 4.22 shows that micron sized alumina particles gave a lower transmittance than nano sized alumina particles.

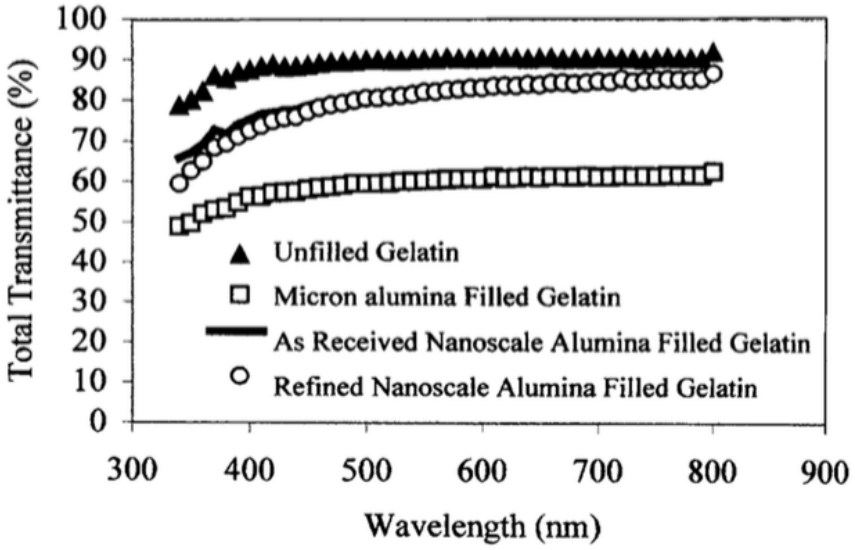

Figure 2.3: Transmittance through gelatin (triangles), gelatin with micron (squares) and nano (circles) sized alumina powder, as a function of wavelength. Retrieved from ref [12].

2.2 Nanomaterials

Since it was first mentioned by Norio Taniguchi in 1974 [13], nanomaterials and nanotechnology have been a topic of great interest for many scientists and researchers. Nanomaterials are known for having different properties compared to their bulk materials counterparts. This is because of the dramatic increase in specific surface area (area divided by mass, $[m^2g^{-1}]$) and quantum effects arising from the confinement at the nanoscale. The mentioned effects are usually observed in the size range of 1 to 100 nm, and The US National Nanotechnology Institute therefore proposed the following definition for nanomaterials in 2004: "*matter at dimensions between approximately 1 and 100* nm*, where unique phenomena enable novel applications*"

[14].

In addition to having different properties compered to bulk materials, nanomaterials also have tuneable properties, as shown in Figure 2.4. Here dispersions of gold nanoparticles with a size of 4 nm show a red colour, while dispersion of gold nanoparticles with a size of 80 nm show a purple colour.

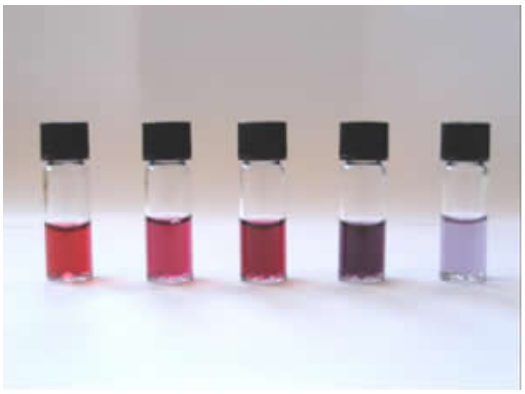

Figure 2.4: Gold nanoparticles of different sizes (4 to 80 nm from left to right) suspended in water, showing different colours.[2]

The extraordinary properties, and the ability to tune these properties, have made nanomaterials interesting for a wide variety of applications. Gas sensors, information storage, fuel cells and drug delivery are a few examples [15].

2.2.1 Finite size effects

Two mechanisms normally effects the properties of materials at the nanoscale, namely scaling and spatial confinement [16].

Scaling effect

The scaling effect arises from the relative increase in specific surface area, i.e. the increase in relative amount of surface to bulk atoms at the nanoscale [16]. Since the volume scales with r^3 while surface area scales with r^2 for a spherical particle with radius r, it can be seen that the relative amount of surface area to volume scales with r^{-1}. Since the chemistry of surface atoms are different from bulk atoms, this increase in surface atoms will change the material properties. Surface atoms have dangling bonds, giving the surface

[2]This picture is reused under the GNU Free Documentation License, Version 1.2 with permission from the copyright holder, Aleksandar Kondinski.

atoms higher free energy, reactivity and mobility. For nanomaterials this means that the melting and evaporation temperature decreases compared to bulk materials, while properties like reactivity, elasticity and plasticity increases. The scaling effect can also lead to phase stabilization of metastable polymorphs, as is the case for TiO_2. For bulk TiO_2, *rutile* (space group $P4_2/mnm$) is the stable polymorph, but for particles smaller than approximately 10 nm (this number is highly dependent on what methods have been used to estimate it, but 10 seems to be in the middle of the range), *anatase* (space group $I4_1/amd$) has been shown to be the most stable polymorph [17]. In Figure 2.5 the potential energy for anatase, rutile and brookite relative to bulk rutile as a function of particle size is plotted, showing that anatase becomes the stable polymorph at around 2.5 nm (0.4 nm^{-1}).

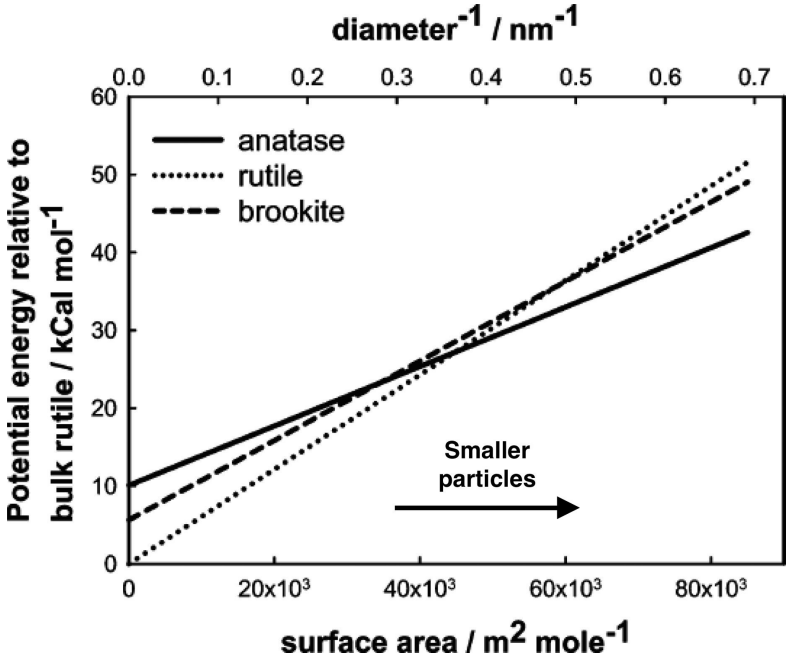

Figure 2.5: Potential energy relative to bulk rutile as a function of inverse particle size for the polymorphs anatase (solid line), rutile (dotted line) and brookite (dashed line). Values retrieved from molecular dynamics simulation at 27 °C. Retrieved from ref [18].

Spatial confinement

Spatial confinement is a result of quantum mechanical effects [16]. In bulk materials these effects are negligible, but at nanoscale these effects start to play a role when the size of a nanosized material is in the same size range

as the relevant length scale for a given material property. For example, the colour of metals arises from an effect called plasmon resonance, which is a collective resonance of the free electrons [16]. The plasmon resonance frequency, i.e. the colour of the metal, is dependent on the electron mean free path (average distance between two consecutive collisions). In bulk gold the mean free path is approximately 50 nm, so when gold nanoparticles have a size around 50 nm, spatial confinement starts to effect the electron free mean path, and then also the plasmon resonance frequency. This gives raise to the change in colour as a function of particle size for colloidal gold nanoparticles, as shown in Figure 2.4.

2.2.2 Synthesis of nanomaterials

For production of nanomaterials, there are mainly two approaches, bottom-up and top-down methods. Top-down methods starts out with a bulk material, and then utilizes grinding or etching to achieve the nanosized material. Top-down methods include different lithography methods, and are heavily used in the semiconductor processing industry [16].

Instead of starting with a bulk material, molecules or atoms can be used as starting point for making nanomaterials, and these methods are called bottom-up methods. By controlling the assembly of atoms or molecules, nanomaterials can be made. Bottom-up methods include sol-gel and hydrothermal synthesis for example. Bottom-up methods are often preferred due to easier up-scaling, and also for the possibility for being cleaner and more environmentally friendly. Where top-down methods use strong acids or volatile gasses, bottom-up methods have the opportunity to utilize water as reaction media for the correct optimization of the process.

Hydrothermal synthesis

Hydrothermal synthesis is widely used for synthesis of nanomaterials, and especially nanoparticles because of its versatility and good crystallinity in the final products. A common definition for hydrothermal synthesis is a chemical reaction carried out in an aqueous media at elevated temperature and pressure [19]. If the reaction media is an organic solvent instead of water, it is called solvothermal synthesis. Both hydrothermal and solvothermal synthesis are carried out by heating the precursors, or chemicals, in a closed vessel called an autoclave, as shown in Figure 2.6. The increased temperature and pressure leads to an increase in solubility and reactivity of the chemicals.

Since a complete understanding of the mechanisms happening during formation and growth of particles under hydrothermal synthesis are not fully

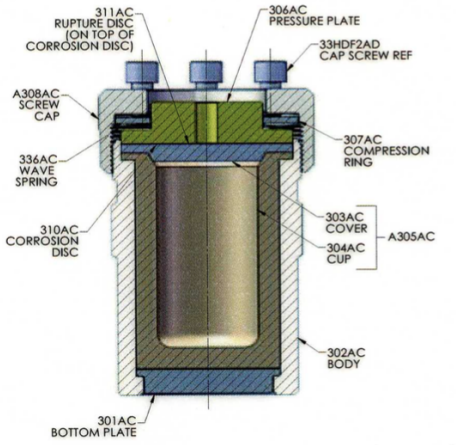

Figure 2.6: Schematic cross section of an autoclave used for hydrothermal synthesis. Retrieved from ref [20].

established, it can be challenging to predict the morphology, size and crystallinity in the final product. Therefore, an individual optimization for each new synthesis route is often needed. Some mechanisms are suggested, and also justified with experiments. They are dissolution and reprecipitation, topotactic transition, oriented attachment and agglomeration [19]. A short description of these mechanisms are found in the author's specialization project [8], and for a more detailed description the reader is referred to the tutorial review by Einarsrud and Grande [19].

2.2.3 Stabilization of suspensions

For synthesis of nanoparticles it is of utmost importance that agglomeration of nanoparticles is controlled. If not, the effective particle size could be much larger than the primary particle size. The driving force for agglomeration is lowering of the Gibbs free energy of the system. Since the surface of materials have higher free energy than the bulk, it is energetically favourable for the particles to agglomerate, lowering the specific surface area. For nanoparticles, with a high specific surface area, this driving force is strong, and thus nanoparticles tend to form agglomerates. There are mainly three ways to avoid agglomeration, all working on colloidal suspensions, namely electrostatic stabilization, surface modification with surfactants and surface functionalization. Common for these methods is that they hinder particle-particle contact, consequently stopping agglomerating.

Electrostatic stabilization

The surface of particles dispersed in water will react with water and form hydroxyl groups on the surface. By changing the pH of the dispersion the surface of the particles can be charged, as illustrated for TiO_2 in Equation 2.7. Ions with opposite charge in the water (H^+ or OH^-) will then electrostatically attract to the surfaces, and form a layer or cloud of charged species around the particles. This phenomena can be measured by setting up a potential across the dispersion, and in a microscope see how the particles move towards the cathode or anode side, depending on the charge. This is known as the ζ-potential.

$$\text{Ti-OH}_2^+ \overset{\text{acid}}{\rightleftharpoons} \text{Ti-OH} \overset{\text{base}}{\rightleftharpoons} \text{Ti-O}^- \tag{2.7}$$

Figure 2.7 shows ζ-potential for TiO_2 as a function of pH. It can be seen that the ζ-potential is 0 mV at pH 6.5, and this is known as the isoelectric point (IEP). Changing the pH away from the IEP will lead to changes indicated in Equation 2.7. As similar charges repels each other, these surface charges can be used to stabilize and suppress agglomeration of nanoparticles in suspensions. A rule of thumb is that the absolute value of the ζ-potential need to be higher than 30 mV to achieve a stabilizing effect. For TiO_2, this means going to pH higher than 8.5. Another rule of thumb is that 3-4 pH units away from IEP will be sufficient for giving a stabilizing effect. Either way, for pure TiO_2 electrostatic stabilization is only possible under acidic or basic conditions. As it is often preferable to work with neutral dispersions, it is desirable to change the surface of TiO_2 so it can be stabilized at neutral conditions.

Surface modification and functionalization

By modifying the surface of the nanoparticles, IEP can be shifted, so that it is possible to achieve a stabilizing effect at neutral conditions. In Figure 2.7 the effect of surface functionalization with 3-aminopropyl-trimethoxysilane (APTMS) on TiO_2 is shown. Equation 2.8 shows a hydrolysis reaction between the silane and water, while Equation 2.9 shows a condensation reaction between the silane and hydroxyl group on the surface of TiO_2, and this is the proposed reaction path for grafting silanes on the surface of TiO_2. The proposed resulting surface is shown in Figure 2.8, where APTMS is grafted and cross linked on the surface of TiO_2 with Ti-O-Si and Si-O-Si chemical bond respectively. A clear shift in IEP towards higher pH values is seen in Figure 2.7, and the IEP is around pH 9, compered to 7 without functionalization. With APTMS grafted to the surface of the particles, TiO_2 have a surface

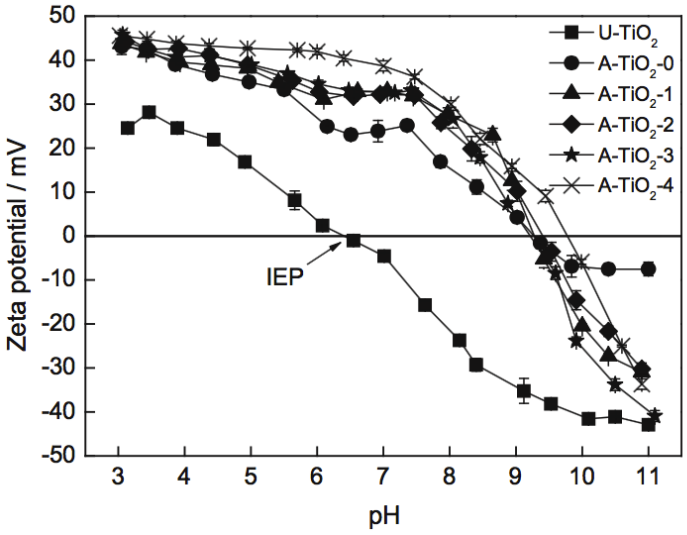

Figure 2.7: ζ-potential for TiO_2 (squares) and TiO_2 functionalized with 3-aminopropyl-trimethoxysilane (APTMS). Retrieved from ref [6].

potential of approximately 30 mV instead of 0 mV at pH 7. This indicates that TiO_2 could be stable at, or close to neutral conditions if functionalized with APTMS or similar grafting agents.

$$RSi(OCH_3)_3 + 3H_2O = 3RSi(OH)_3 + 3CH_3OH \tag{2.8}$$

$$RSi(OH)_3 + HO\text{-}TiO_2 = RSi(OH)_2\text{-}O\text{-}TiO_2 + H_2O \tag{2.9}$$

Similar to surface functionalization is the use of surfactants. Although no chemical reaction occur between the surface and molecule, the molecule still adsorbs to the surface. Figure 2.9 shows how the surfactant sodium-dodecyl-sulfate (SDS) lowers the ζ-potential of TiO_2 in water and dodecyldimethy-lamine oxide (C_{12}DAO) increases it. It can be seen that the ζ-potential is lowered from approximately 0 to -50 mV at pH 7 with SDS. This means that a stabilizing effect can be achieved at pH 7 for TiO_2 by addition of SDS.

2.2.4 De-agglomeration

Often, nanoparticles will need to be de-agglomerated before they can be stabilized with one of the methods mentioned above. Two methods often used are ultrasonification and milling.

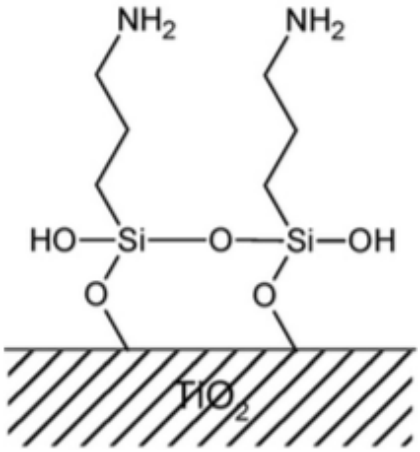

Figure 2.8: Schematics of how 3-aminopropyl-trimethoxysilane (APTMS) molecules are believed to graft and crosslink on the surface of TiO_2. Retrieved from ref [6].

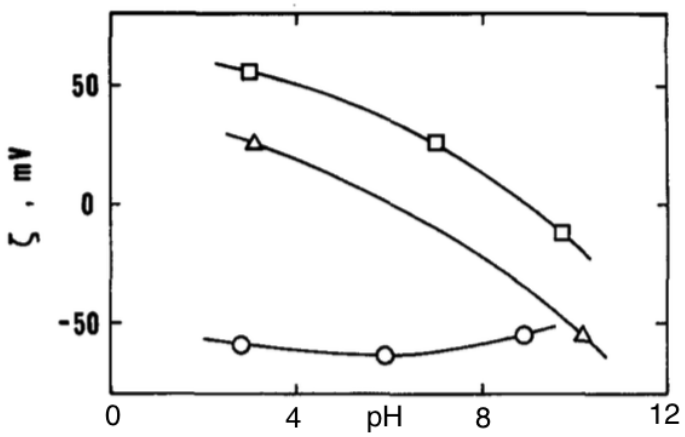

Figure 2.9: ζ-potential for TiO_2 (triangles) and TiO_2 with surfactants SDS (circles) and C_{12}DAO (squares). Retrieved from ref [5].

Ultrasonification

Ultrasonification means to expose a suspension to a mechanical wave (high intensity sound waves) with relatively high frequency. These mechanical waves will result in pressure differences in the liquid, and cavities or bubbles will form and collapse in a continuous cycle. The collapsing bubbles give rise to a phenomena called cavitation. The collective collapse of bubbles releases energy in forms of mechanical stirring, shock waves and micro-jets that can break down agglomerates [21]. In the work done by Sauter *et al.* [21] the

effect of wave amplitude and time used for ultrasonification is investigated. They find no significant effect of amplitude but observe that longer times (up to 20 min) gives smaller agglomerates. It should be mentioned that their primary particle size is 12 nm, and after ultrasonification for 20 min the particle size is still over 170 nm, indicating that the particles are still agglomerated.

Milling

Milling can be done in several ways, and ball milling as shown to the left in Figure 2.10 is perhaps the simplest form. The ball mill consist of a cylinder filled with grinding media (balls/beads, short cylinders or rods), and by rotation of the cylinder the grinding media will crush the particles or powder that is milled. By controlling filling factor of the cylinder, ball sizes (20-1 mm in diameter), morphology of the milling balls and rotation speed, particle sizes of 5 µm or smaller can be achieved [22]. Attrition milling shown in the middle of Figure 2.10 is another milling method. Instead of rotating the whole cylinder for moving the grinding media, a rotating shaft with arms is rotated. Attrition milling is known to be faster, give smaller particle sizes and less contamination than ball milling [22]. Both ball and attrition milling can be done dry, or wet. Some advantages with wet over dry is that smaller particles and narrower size distribution is achieved [22].

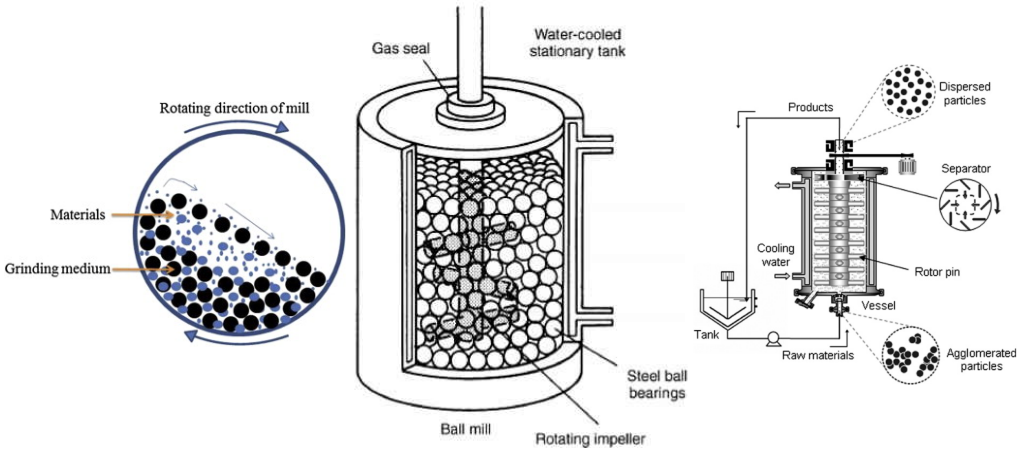

Figure 2.10: Schematic of ball mill (left), attrition mill (middle) and modified attrition mill described by Inkyo *et al.* [23] (right). Left and middle figure is retrieved from [24] and [25] respectively.

For achieving particle sizes smaller than a few hundred nanometers, more specialized milling methods must be used. Such a setup is shown to the right

in Figure 2.10. This setup is similar to an attrition mill working in wet mode, but the size of the milling balls used is as small as 15 μm. This setup has reported to break agglomerates down to primary particle size of 15 nm [23].

2.3 Nanoparticle composites

The term nanoparticle composite, or nanocomposite, have for the last decades received increasing interest because of their many interesting properties. The technology itself is ancient, going back to the late Bronze age (1200-1000 BC), where copper nanoparticles were used for achieving red coloured glass [26]. Of course, at the time they only knew the process, but with techniques like scanning and transmission electron microscopy, we can today investigate archaeological founds from that time period and see the copper nanoparticles in the glass.

In more recent time, Toyota is considered to be the first company to commercialize nanocomposites with their patent in 1988 [27]. They patented a composite material with "*high mechanical strength and excellent high-temperature characteristics*" [27], consisting of a polyamide matrix with uniformly dispersed thin sheets of aluminum or magnesium phyllosilicate (a type of clay).

Still, it is not until more recent time that knowledge and technology have made it possible to tailor a wide variety of nanocomposites. By utilizing the easy formability of polymers and the unique properties of nanoparticles, polymer-nanoparticle composites have become an interesting material class for optical, mechanical, electrical, magnetic and fire retardancy applications [28].

The big challenge working with polymer-nanoparticle composites is to achieve homogeneously dispersed particles in the matrix. And as stressed earlier, this challenge gets even more challenging when working with nanoparticles of an inorganic material. This is because of the big difference in surface energy (around 50 mJm^{-2} and 500 mJm^{-2} for polymers and inorganic materials respectively). It is therefore much more energetically favourable for the system to cluster the nanoparticles together to reduce their surface area, than it is to have them well dispersed in the polymer matrix.

2.4 Literature review

2.4.1 Hydrothermal synthesis

Hydrothermal synthesis has been extensively used for making TiO_2 nanoparticles. Different TiO_2 precursors have been used, and different reaction conditions have been investigated.

Zhang *et al.* [29] used $TiCl_3$ and $TiCl_4$ as TiO_2 precursor in different ratios. By changing the $TiCl_3$:$TiCl_4$ ratio they found that they could tune the phase composition in the final product, from pure mono-phase rutile, to bi-phase anatase and rutile and further to tri-phase anatase, bookite and rutile. The morphology was also influenced by the ratio of $TiCl_3$ and $TiCl_4$, where high amounts of $TiCl_3$ gave rodlike particles. This was argued to be caused of the slower reaction rate of Ti^{3+} (needs to be oxidized to Ti^{4+} to form TiO_2) compared to Ti^{4+}.

A more common precursor is titanium (IV) isopropoxide (TIP). Hayashi and Torii [30] investigated the effect of reaction time (2, 8 and 24 h) and temperature (100, 200, 300 and 400 °C) on TiO_2 produced from a TIP precursor mixed with water. They report an increase in crystallite and particle size with increasing time and temperature. In the work by Dalod *et al.* [7] the same synthesis route as Hayashi and Torii is used, with the modification of adding different silanes to the reaction with the goal of achieving *in situ* functionalization of the final particles. They reported successful synthesis of *in situ* functionalized TiO_2 nanoparticles for all three silanes investigated, and they observed an elongation of particles when synthesized with amino silane. This was argued to arise from a combination of selective attachment of amino silane, and oriented attachment of particles. In the authors spesialization project [8] the work by Dalod *et al.* was continued, and the effect of shorter reaction times on the elongated particles were investigated. The results show that shorter reaction time supresses the formation of elongated particles.

Barbé *et al.* [31] used TIP mixed with water to investigate the growth of anatase nanoparticles under different hydrothermal conditions. They show that the particle growth is affected by temperature, where higher reaction temperature gives slightly larger particles. Bigger particles are also obtained with basic reaction conditions (ammonia, pH=11) compared to acidic reaction conditions (nitric acid, pH=1), where the average particle sizes calculated from BET surface areas are 20 and 14.5 nm respectively. They also report that sedimentation occured during the hydrothermal synthesis, and an ultrasonic horn was used to disperse the particles after synthesis. Chae *et al.* [32] used TIP in an acidic (nitric acid, pH=0.7) water and ethanol mixture,

and investigated the effect of water ethanol ratio, and TIP concentration. They report that an increased amount ethanol gives smaller particles (down to 7 nm), and for a fixed ethanol water ratio, smaller particles are obtained by increasing the TIP concentration. Chae *et al.* also report that the synthesized particles were obtained as a stabile colloidal suspension, where particle size distribution show agglomerates with a size of 40 nm for the smallest particles. This is probably because of the very acidic environment, giving strong electrostatic stabilization, that hinders agglomeration.

Penn and Banfield [33] investigated the growth and morphology development under hydrothermal conditions of anatase nanoparticles (around 5 nm) made from a sol-gel process. They found that different crystallographic faces of anatase grew at different speeds at different time intervals during synthesis. Up to 25 h growth along the [001] direction is the fastest growing direction. This effect is suppressed by addition of HCl.

A small overview of work done on hydrothermal synthesis is shown in Table 2.1, with some featured reaction conditions and key results.

2.4.2 Stabilization of suspensions

As suggested in the work done by Barbé *et al.* [31], special effort is often needed to achieve a stable dispersion of nanoparticles syntheized by hydrothermal synthesis. Several approaches have been used for achieving a stable dispersion, including electrostatic stabilization, surface modification with surfactants and surface functionalization with a grafting agent. Here follows an overview of some of the work done with respect to surface functionalization.

Grafting with silane

In the work done by Iijima *et al.* [35] it is shown how the right amount of grafting agent can give well dispersed nanoparticles, with an effective size close to the primary particle size. This is done by titrating a diluted mixture of APTMS and decyltrimethoxysilane (DTMS) into an acidic water methanol dispersion containing well dispersed TiO_2 nanoparticles, and then stirring for 16 hours. By changing the ratio between APTMS and DTMS they show that it is possible to tune the dispersibility in different solvents by changing the overall hydrophobicity of the particles. Sabzi *et al.* [36] grafts TiO_2 with APTMS with a reflux technique using toluene, and shows how this gives improved dispersibility and mechanical properties in a polyurethane coating compared to untreated particles. Ukaji *et al.* [37] reports that TiO_2 nanoparticles functionalized with 3-aminopropyl-triethoxysilane (APTES) have an

Table 2.1: Overview of reaction conditions used for hydrothermal synthesis of TiO_2 nanoparticles, and key results from literature.

Author	Temperature [°C]	Time [h]	pH	Reaction media	Key result
Barbé *et al.* [31]	200-250	12	1 and 11	Water	Basic con. gives larger particles than acidic con.
Chae *et al.* [32]	150-300	4	0.7	Water Ethanol	Particle size decreased with amount of ethanol
Hayashi and Torii [30]	100-400	2-24	N/A	Water	Particle size increased with temp. and time
Penn and Banfield [33]	100-250	1-255	N/A	Water	Rapid growth in the [001] direction
Horvat *et al.* [34]	40-200	50-150	N/A	Water	Particle size increased with temp. and time
Dalod *et al.* [7]	200	2	N/A	Water silane	*In situ* functionalized particles, elongation with amino silane
Grendal [8]	200	0.25-2	N/A	Water amino silane	Elongation of amino silane functionalized particles supressed by shorter time

increased UV-shilding ability while the photocatalytic effect is suppressed. This is done by dispersing the particles in *o*-xylene, add APTES before continues stirring for 6 h in a 50 °C oil bath. Suppressed photocatalytic effect is very beneficial in many applications, as high photocatalytic effect can lead to faster decomposition. Zhao *et al.* [6] have done a thorough investigation of the reaction happening between the surface of TiO_2 and silane coupling agents, and proposed the reaction path as shown in Equation 2.8 and 2.9.

The methods discussed so far are all examples of *post* functionalization, meaning the particles are synthesized, and then functionalized. Functionalization have also been shown to be possible *in situ*, meaning that the particles are synthesized and functionalized in the same process. Koziej *et al.* [38] uses a solvothermal method to make TiO_2 nanoparticles grafted with 3-trimethoxysilyl-propyl methacrylate for use in a UV-absorbing transpar-

ent poly(methyl methacrylate) (PMMA) film. They report that the functionalized particles show better dispersion in the film compared to unfunctionalized particles. They also report an increase in particle size with 3-trimethoxysilyl-propyl methacrylate compared to synthesis of unmodified TiO_2. This is similar to what was reported by Dalod *et al.* [7], where elongated rod like particles appeared when particles were functionalized with amino silanes (APTES and 3-(2-aminoethylamino)-propyldimethoxymethyl silane (AEAPS)) in a hydrothermal synthesis. This was in contrast to the smaller and more spherical particles observed when functionalized with n-decyltriethoxysilane (DTES), in the same work by Dalod *et al.*

From this it is clear that in addition to having the potential for stabilizing nanoparticles, surface functionalization with silanes can also be used to improve wanted, or suppress unwanted properties, and to achieve good dispersibility in a wide variety of solvents. Surface functionalization looks like a promising way to achieve good dispersibility of nanoparticles in a polymer matrix.

2.4.3 Polymer-nanoparticle composite

The big challenge with polymer-nanoparticle composite, especially when working with inorganic nanoparticles, is to achieve a homogenous dispersion of particles in the polymer matrix. A lot of work has been done in this field, and several approaches have been successful in production of polymer-nanoparticle composites.

Zhao and Li [39] show how nanoparticles can be dispersed in polypropylene (a thermoplastic, i.e. it can be melted and be mouldable above a given temperature) by mixing nanoparticles with polypropylene pellets in a twin screw extruder. They report that this gave a good dispersion of nanoparticles, and that the nanoparticles gave significant improvement on the photodegradation resistance of polypropylene to UV-irradiation. Li *et al.* [40] investigated the effect of ZnS nanoparticles in a UV-shielding, high transparency epoxy film. The epoxy consisted of a curing agent and the epoxy. Li *et al.* dispersed the nanoparticles in the curing agent using ultrasonification before adding the epoxy, before necessary heat treatment. A high transparency and UV-shielding epoxy was obtained from this method. Cheng *et al.* [41] reported that they were able to evenly disperse as much as 30 wt% ZnS nanoparticles into a N,N-dimethylacrylamide, styrene and divinylbenzene polymer by what they call an *in situ* bulk polymerization. This was done by dispersing ZnS in N,N-dimethylacrylamide at 75 °C, before styren, divinylbenzene and the polymerization initiator, azobisisobutyronitrile, were added. The film showed high transparency and an increase in refractive

index.

In addition to use heat or ultrasonification for dispersing the nanoparticles, both Zhao and Li [39] and Cheng *et al.* [41] stresses the importance of using functionalized nanoparticles for achieving a good and homogenous dispersion.

Chapter 3

Experimental

3.1 Synthesis of TiO_2 nanoparticles

The chemicals used for synthesis of TiO_2 nanoparticles are shown in Table 3.1. Titanium (IV) isopropoxide (TIP) and 3-aminopropyl-triethoxysilane (APTES) react strongly with air and must therefore be handled in a glove box with inert atmosphere, or with a septum on the chemical bottle to avoid unwanted reactions of the chemicals. Normal precautions for working with acids and bases must be taken when working with nitric acid and ammonium hydroxide. Preparations for the synthesis should be done in a fume hood, if not in a glove box.

All synthesis were carried out with a filling factor of 70 % of the PTFE cup (Parr, 125 ml). This was achieved by always using 8 ml of TIP, and then calculating the desired amount of amino silanes depending on the wanted TIP:APTES molar ratio (10:1 and 15:1). The rest of the volum needed to

Table 3.1: Overview of the chemicals used for synthesis of *in situ* functionalized TiO_2 nanoparticles.

Chemical	Abbreviation	Purity [%]	Supplier
Titanium (IV) isopropoxide $Ti(OCH(CH_3)_2)_4$	TIP	97	Sigma-Aldrich
3-aminopropyl-triethoxysilane $C_9H_{23}NO_3Si$	APTES	99	Sigma-Aldrich
Nitric acid HNO_3	N/A	65	Sigma-Aldrich
Ammonium hydroxide NH_3 (aq)	N/A	30-33	Sigma-Aldrich

achieve 70 % filling factor was filled with distilled water. The volum of nitric acid and ammonium hydroxide were assumed negligible for the synthesis were used, since only a few drops were needed to achieve the wanted pH.

A normal synthesis was performed as explained in the following. Distilled water was measured with a measuring sylinder and poured into a beaker. Since the amount of APTES was small, a scale was used for better accuracy. APTES was added drop by drop to the beaker while placed on a scale before the APTES water mixture was placed on a magnetic stirrer. TIP was then measured out using a syringe, and as quickly as possible after removing the needle from the septum, was added to the APTES water mixture. A white precipitate formed immediately, and the dispersion was stirred for 10 min at room temperature. For synthesis carried out at acidic or basic conditions the pH was adjusted by adding nitric acid or ammonium hydroxide after the stirring ("neutral" conditions would be pH 4.4 and 6.3 for synthesis without and with APTES respectively). pH was measured before and after addition of acid or base with a Mettler Toledo SevenEasy S20 pH meter. A two-point-calibration at pH 4 and 7 was always done before measuring. Then the dispersion was poured into the PTFE cup, and all residues were scooped out using a spatula. The autoclave was assembled and placed in a Fermacks T8000 Series drying oven. The autoclave was cooled to room temperature in the oven.

Table 3.2: Reaction times, temperatures, pH and amount of amino silane used in the synthesis of *in situ* functionalized TiO_2 nanoparticles.

Sample/short name	Molar ratio TIP:Silane	Temperature [°C]	Time [min]	pH
Ti-acidic	N/A	200	120	2.7
Ti-basic	N/A	200	120	9.3
10:1-acidic	10:1	200	120	2.2
15:1-acidic	15:1	200	120	2.2
10:1-150 °C	10:1	150	120	6.3
15:1-150 °C	15:1	150	120	6.3
10:1-1 min	10:1	200	1	6.3
15:1-1 min	15:1	200	1	6.3
10:1-basic	10:1	200	120	10.1
15:1-basic	15:1	200	120	9.7
10:1-ref	10:1	200	120	6.3
15:1-ref	15:1	200	120	6.3
Ti-ref	N/A	200	120	4.5

Table 3.3: Overview of the chemicals used for dispersion of TiO_2 nanoparticles.

Chemical	Abbreviation	Purity [%]	Supplier
Diethyl ether $(C_2H_5)_2O$	N/A	99.7	Sigma-Aldrich
Xylene $C_6H_3(CH_3)_2$	N/A	N/A	Sigma-Aldrich
Sodium dodecyl sulfate $CH_3(CH_2)_{11}SO_4Na$	SDS	N/A	Sigma-Aldrich
P53 Silicon-based polymer	P53	N/A	poLight

After room temperature was reached the mixture from the PTFE cup was centrifuged (10000 rpm for 10 min) three times. After each centrifugation the fluid was poured off while keeping the sediments, and distilled water was then added. Vigorous manual stirring in the centrifugation tubes with a spatula was done after adding distilled water to remove any unreacted or unwanted produced chemicals (mainly APTES and propanol). Half of the sample was then dried on a watch glass at 120 °C over night before it was grinded. The other half was kept in distilled water. An overview of the samples prepared as a part of this work is shown in Table 3.2. The structure of the short name is A-B where A stands for molar ratio of TIP:APTES (10:1 or 15:1) or Ti indicating no APTES, and B indicates the characteristic parameter for that synthesis. B is then relative to the samples named A-ref. The three samples named A-ref were prepared as a part of the authors specialization project [8], and are included here for comparison. The A-ref samples were prepared without adjusting the pH at 200 °C for 120 min. The samples prepared as a part of this work only varies with one parameter from the respective A-ref sample.

3.2 Dispersion of TiO_2 nanoparticles

Several approaches were used for achieving stable dispersions of TiO_2 nanoparticles. *In situ* functionalization was one approach, but will not be further explained here, as that is thoroughly explained in Section 3.2. The other approaches used is shown in Figure 3.1. Four approaches was used, as indicated by the colour and letter coding in Figure 3.1. All the chemicals used are listed in Table 3.3, and all ultrasonification was done using a Branson Digital Sonifier finger.

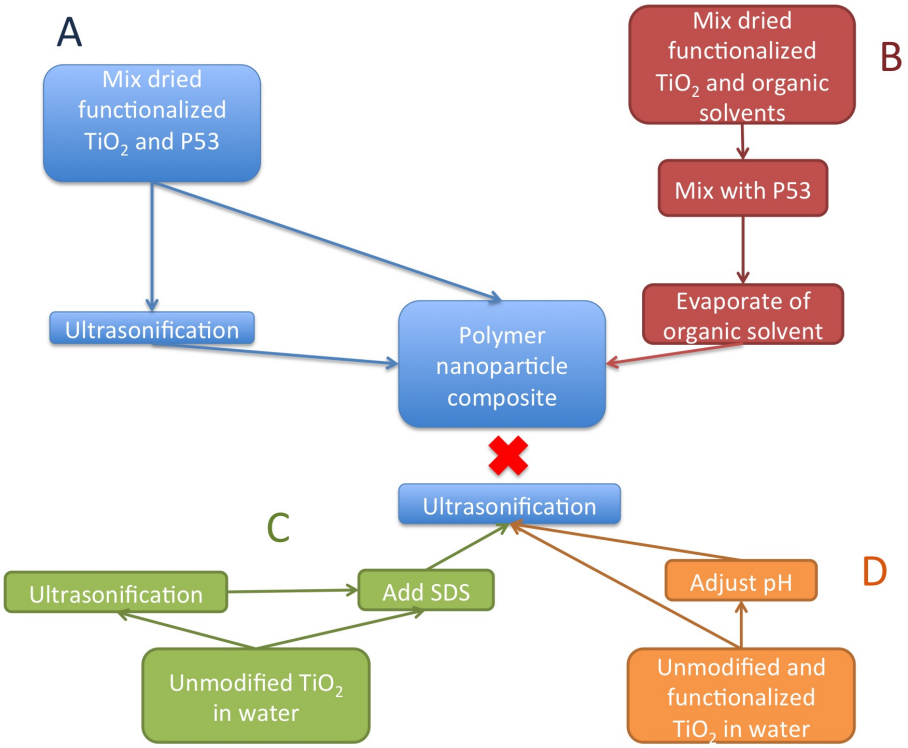

Figure 3.1: Flowchart showing the different approaches used for making a stable dispersion of de-agglomerated TiO_2 nanoparticles. Red cross indicating that no composite was made from this approach.

The approach indicated by a A (blue colour) was done by mixing dried particles (1vol%) (particles used are indicated in Table 3.4) and the polymer in a sample glass, and then manually stirring the mixture with a spatula. Ultrasonification was done with amplitudes ranging from 30-70 % for 5 sec to 1 min.

Approach B (red colour) was done by first mixing dried particles (1vol%) with one of the organic solvents, diethyl ether or xylene. No ultrasonification was done because both solvents are highly flammable. The mixture was then mixed with the polymer and placed on a combined magnetic stirrer and hot plate to evaporate away the organic solvent. Only diethyl ether evaporated in a reasonable time, so diethyl ether was used when making the composite from this approach.

Making a stable dispersion with surfactants was also tried as indicated by the approach marked C (green colour). Sodium dodecyl sulfate (SDS) was added to a dispersion of unmodified TiO_2 in distilled water. Ultrasonifi-

cation was applied before and after adding SDS. For ultrasonification before addition of SDS, both an investigation of the solid:liquid (TiO_2:distilled water) ratio and longer exposures to ultrasonification was done. Dispersions containing 1, 0.1 and 0.01 wt% TiO_2 was prepared for the investigation of solid:liquid ratio, and ultrasonification for 10 min at 50 % amplitude was used. Longer exposures of ultrasonification was investigated by dispersing unmodified TiO_2 (1vol%) in water, and using ultrasonification for 10 to 20 min at 50 % amplitude.

Adjusting pH was tried to achieve electrostatic stabilization, as indicated in the approach marked D (orange approach). Both modified and unmodified particles (1wt%) were dispersed in distilled water, and then the pH was adjusted by addition of nitric acid. pH was measured to be between 7 and 6 before, and 2 and 1 after addition of nitric acid with pH-paper.

3.3 Synthesis of polymer-nanoparticle composite

The specifics about the preparation of P53 are company secrets and can therefore not be explained here. A reference of P53 without particles was prepared on a glass slide by drop casting. Drop casting on glass slides was utilized for polymer films with particles as well, after mixing polymer and particles. Volume percent, particles used and the dispersion approach used for the samples made are shown in Table 3.4. The short names are structured as A-B, where A indicates the volume percent of particles, and B is the short name of the particles used.

Table 3.4: Particle concentration, particle and dispersion approach used for preparation of polymer-nanoparticle composites.

Sample/short name	Particle concentration volume percent [%]	Particle	Dispersion approach
Pure-P53	N/A	N/A	N/A
0.5vol%-10:1-15 min	0.5	10:1-15 min*	B, red
1vol%-10:1-15 min	1	10:1-15 min*	A, blue
5vol%-10:1-acidic	5	10:1-Acidic	A, blue
5vol%-Ti-acidic	5	Ti-Acidic	A, blue
15vol%-10:1-acidic	10	10:1-Acidic	A, blue
15vol%-Ti-acidic	10	Ti-Acidic	A, blue

*This sample was prepared as a part of the authors spesialization project [8].

3.4 Characterization

3.4.1 TiO_2 nanoparticles

Phase purity and composition

X-ray diffraction (XRD) (D8 Advance Da-Vinci working in Bragg-Brentano geometry (2θ-θ)) was used to investigate the particles phase purity and composition. All samples were scanned from 2θ=15 to 75° for 30 min using a varying slit (V6). Rietveld refinement in the software *Topas* version 5 was used to estimate the crystallite sizes of the particles and phase composition.

Preparation of the samples was done by taking a small amount of powder on a silicon wafer, before a few drops of ethanol was added. The particles were homogeneously distributed on the silicon wafer by careful rotational tilting of the wafer before the ethanol dried.

Particle size, size distribution and morphology

Particle size and morphology were investigated on an in-lens cold field emission Hitachi S-5500 S(T)EM. Secondary electrons at 7 kV were detected. The line-interception method counting over approximately 100 particles was used to estimate particle size. Samples were prepared by letting a very diluted dispersion of particles in distilled water dry on the sample holder (4 to 24 h, longer drying time gave higher quality pictures). No further sample preparation was then needed, if the dispersion was sufficiently diluted.

A Horiba LA-960 Laser Particle Size Analyser working in wet mode was used for measuring the particle size distribution. Distilled water was used as carrier fluid.

Specific surface area and pores

Adsorption and desorption of nitrogen was measured using a Micrometrics Tristar 3000, and specific surface area and average pore diameter were estimated using BET and BJH method respectively. The samples were degassed for approximately 12 h at 180 °C in vacuum to remove moisture before measurements. By assuming spherical and non-porous particles the particle sizes were calculated from BET specific surface area.

Grafting of amino silanes

The amount of grafted amino silane was investigated by thermogravimetric analysis (TGA) on a Netzsch Jupiter STA 449 C using synthetic air. To

remove adsorbed water the particles were heat treated from 25 to 150 °C (10 °C min^{-1}), hold at 150 °C for 30 min and then heated from 25 to 200 °C (2 °C min^{-1}). Then the samples were heat treated from 100 to 700 °C (2 °C min^{-1}), see Figure 3.2 for the complete heating procedure. Average surface coverage (molecules nm^{-2}) was calculated using Equation 3.1, as done by García-González *et al.* [42].

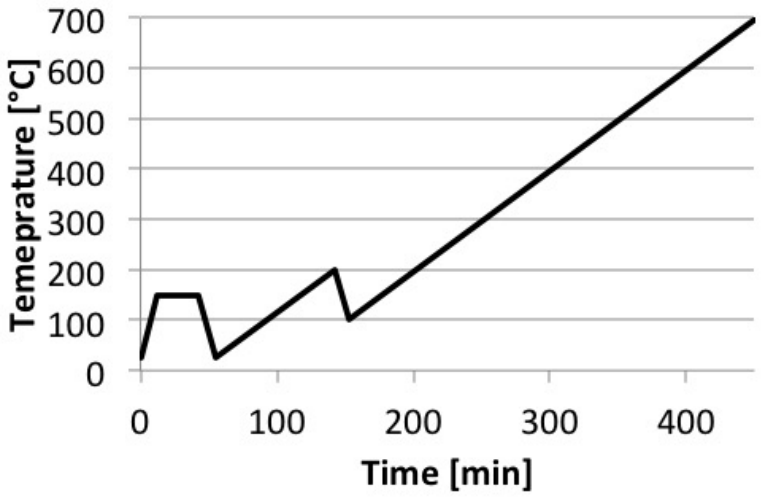

Figure 3.2: Complete heating procedure used to investigate the amount of grafted amino silanes by TGA.

$$\text{Surface coverage} = \frac{d_s \cdot N_A}{M \cdot a_s} \tag{3.1}$$

In this equation d_s ([-]) is the relative mass loss due to amino silane burn off, N_A ([mol^{-1}]) is Avogadros constant, M ([g mol^{-1}]) is the molar mass of what is burnt off and a_s ([nm^2g^{-1}]) is the specific surface area. In the calculations it is assumed that only the carbon chain with the amino group is burnt off, and the rest of the amino silane is still on the particle surface, see Figure 2.8, giving M=58 g mol^{-1}. The samples respective specific surface areas from BET analysis were used as value for a_s.

In addition to TGA, Fourier transformed infrared spectroscopy (FTIR) was used to investigate the chemical bonds on the particles surface. Spectras were acquired on a Bruker Vertex 80v used in ART mode from 600 to 4500 cm^{-1} in air. A total of 32 scans were taken for each sample, with a resolution of 1 cm^{-1}. For best results, a background scan was acquired before each sample to counter the build up of CO_2 and water vapour in the sample chamber due to the operators breath when cleaning and changing samples.

FTIR spectra were also acquired for the samples prepared as a part of the authors specialization project.

3.4.2 Polymer-nanoparticle composite

Refractive index

Refractive index was measured as a function of wavelength (200 to 1700 nm) on a RC2 vertical ellipsometer from J.A. Woollam Company. The measurements were done at 65° angle to the incident beam. The setup was calibrated using a Si-wafer and fitting the measured data with a model in *CompleteEASE* version 5.13 sofware. Fitting the data for the polymer was not possible, so the measured values are to be interpreted relative to each other, and not as absolute values. No sample preparation was done after synthesis for these measurements.

Transmittance

Transmittance was measured on an Olis 14 UV/VIS/NIR Spectrophotometer from On-Line Instruments Systems as a function of wavelength (300 to 1000 nm). Numbers of increment and reads per datum was 175 and 10 respectively. A double baseline (doing a second baseline with the first baseline as baseline should give 100 % transmittance) scan was performed to ensure that the instrument was ready for measurements. Samples was measured without any further sample preparation after synthesis.

E-modulus

Atomic force microscope (AFM), a Veeco MultiMode 8, with *Peak Force Quantitative Nanomechanical Mapping* (QNM) was used for measuring the E-modulus of the pure polymer and composites. Peak Force Quantitative Nanomechanical Mapping is a method developed by Bruker Corporation which uses the adhesion force curve (the force, as a function of distance between AFM-tip and sample surface, acting on the AFM-tip/cantiliver as the tip is removed from the sample surface) to calculate the E-modulus of the sample.

Calibration and measurements was conducted as explained in the Peak-Force QNM user guide from Bruker [43]. This means calibrating *deflection sensitivity*, *spring constant* and *tip radius*. Deflection sensitivity was done with a sapphire calibration sample and the spring constant was found using thermal tune. The tip radius was found using the relative method, meaning a calibration sample with a known E-modulus was used, and then the tip

Table 3.5: Overview of AFM-tips used for Peak Force QNM.

Name	Spring constant (nominal) [Nm^{-1}]	Tip radius (nominal) [nm]	Material	Supplier
MLCT	0.01	20	Si_3N_4	Bruker Corp.
SNL-10	0.06	2	Si_3N_4	Bruker Corp.

radius was set to that value giving the correct E-modulus for the calibration sample. The value for the tip radius was then checked to be a reasonable value compared to the nominal value given from the manufacturer. The last important parameter to adjust was *Peak Force Amplitude*. This value controls the amplitude the tip oscillates in. If set to low working with an adhesive sample, the tip may never disconnect from the sample, and the adhesion force curves will not be representative for the sample. Typical values used was 300 nm.

Two different AFM-tips were tested in the process of optimizing the procedure for achieving good measurements, and their specifications are shown in Table 3.5.

Chapter 4

Results

4.1 TiO_2 nanoparticles

4.1.1 Particle size and morphology

SEM images of Ti-acidic and Ti-basic are shown in Figure 4.1, and Figure 4.2 and 4.3 show SEM pictures of samples with 10:1 and 15:1 molar ratio respectively. For Ti-acidic and Ti-basic small spherical particles are observed, and compared to Ti-ref small to no change is observed as a result of the different reaction conditions. Ti-basic appear slightly bigger and more faceted than Ti-acidic, and this is also confirmed with the particle sizes estimated from line interception that is presented in Table 4.1. The particle size of Ti-basic is 9.1 nm compared to 7.9 nm for Ti-acidic.

For the samples with 10:1 molar ratio bigger changes is observed. 10:1-ref contains the same small spherical particles as the samples without amino silane, but also some bigger elongated particles. For the samples 10:1-1min, 10:1-150 °C and 10:1-acidic the elongated particles are gone, while for 10:1-basic, the elongated particles appears to be bigger and in greater number. For the samples with 15:1 molar ratio a similar trend as for 10:1 molar ratio is observed. For 15:1-1min and 15:1-150 °C the elongated particles observed for 15:1-ref are gone. The same clear difference between 10:1-basic and 10:1-acidic is not observed for 15:1-basic and 15:1-acidic, where both samples consist of a mix of elongated particles and small spherical particles.

All calculated particle sizes are shown in Table 4.1. As observed in the pictures, 10:1-basic have the largest particles (13.7 nm), and is significantly bigger than the particle size of 10:1-acidic (8.3 nm) and 10:1-ref (11.6 nm). The smalest particle size calculated is for 10:1-1min with 7.2 nm. It should be noted that all samples consist of what appears to be non-porous particles.

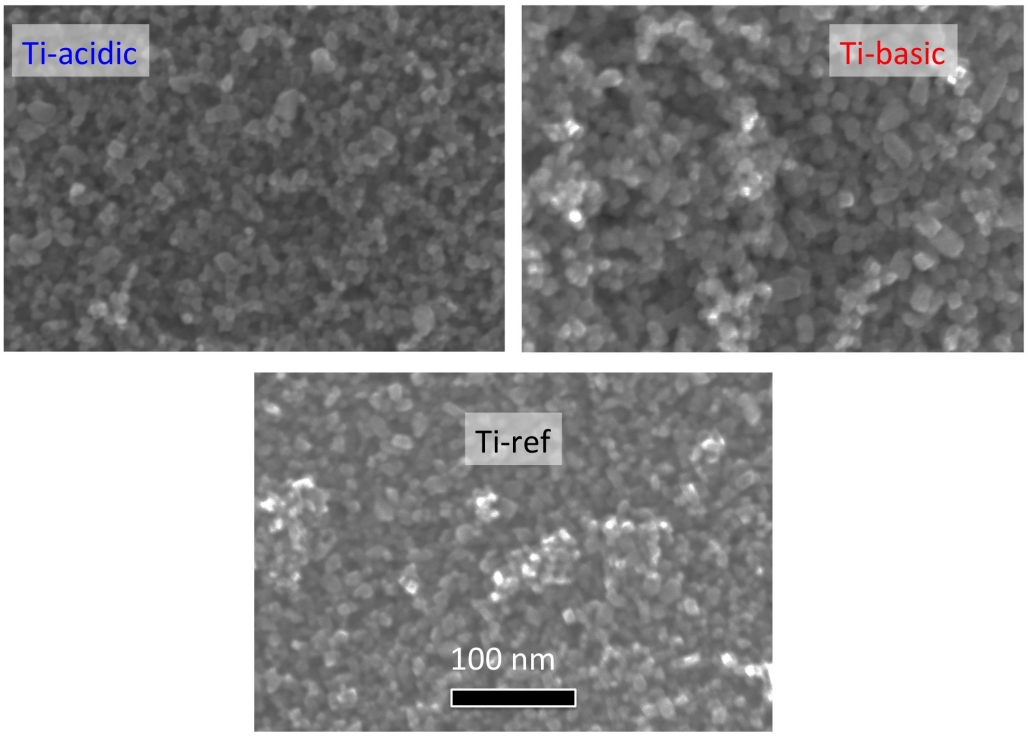

Figure 4.1: SEM images of unmodified TiO_2 nanoparticles prepared with acidic, basic and neutral conditions. All images have the same scale bar.

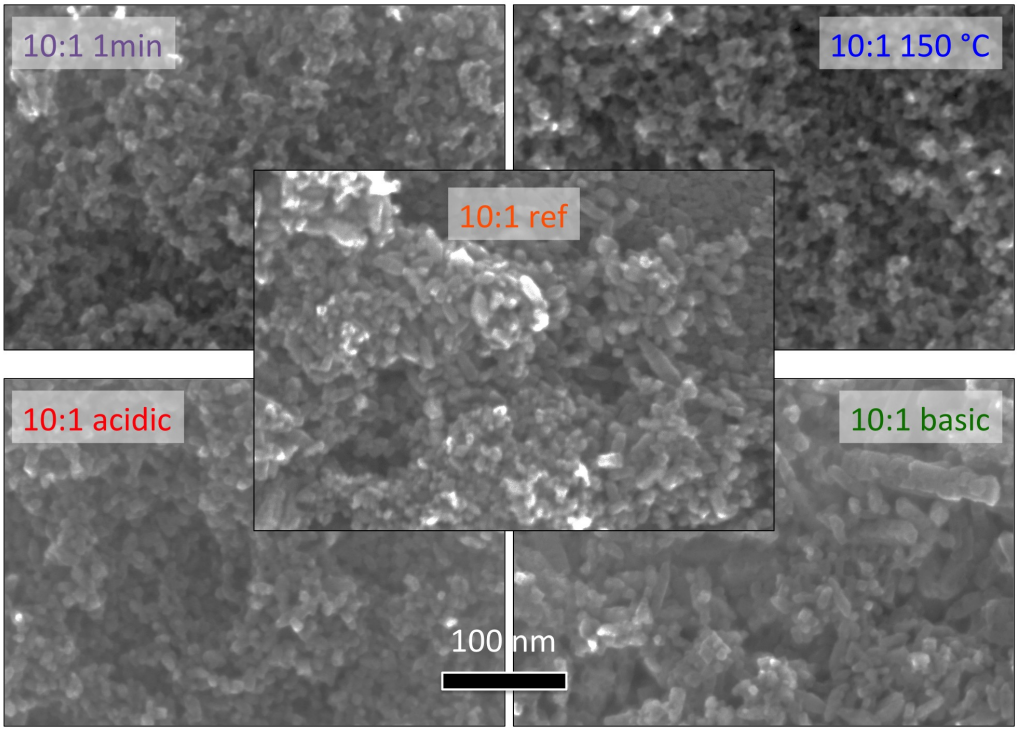

Figure 4.2: SEM images of samples with 10:1 molar ratio at different reaction conditions. All images have the same scale bar.

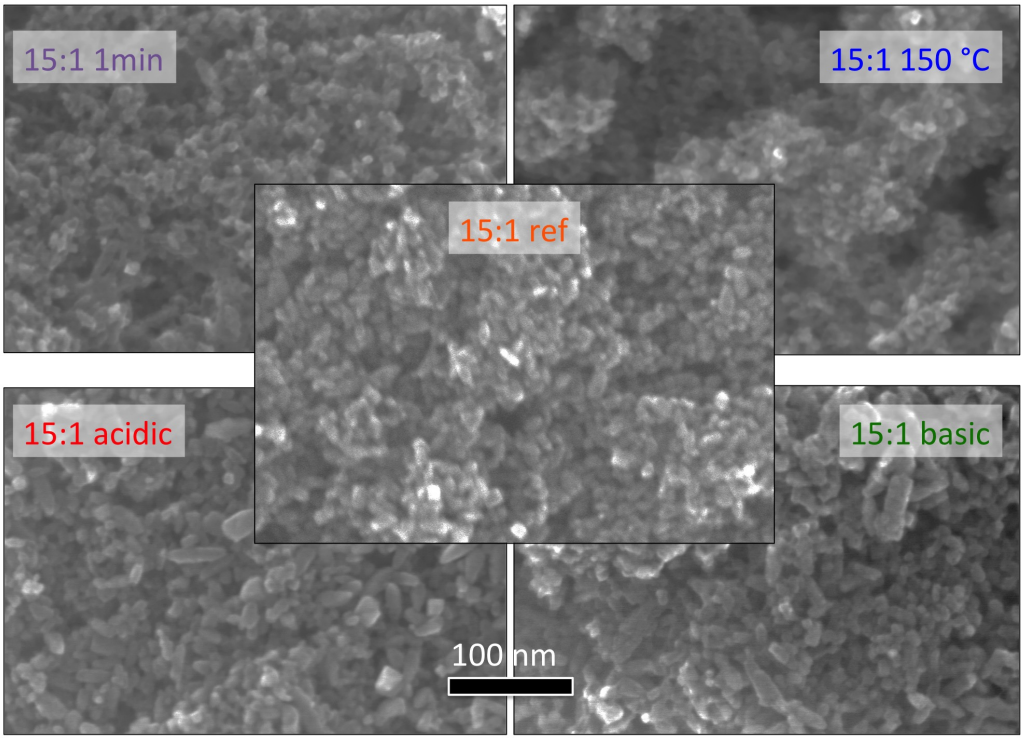

Figure 4.3: SEM images of samples with 15:1 molar ratio at different reaction conditions. All images have the same scale bar.

4.1.2 Phase purity, composition and crystallinity

X-ray diffractograms are presented in Figure 4.4, 4.5 and 4.6 for samples with pure TiO_2, 10:1 and 15:1 molar ratio respectively. From Figure 4.4 it can be seen that the samples prepared without amino silane are mostly anatase (shown with bars), but also contains some brookite (shown with an asterisk). By Rietvield refinement the brookite amounts was estimated for Ti-acidic, Ti-basic and Ti-ref to be 31, 17 and 25 % respectively. The broad diffraction peaks indicate small crystallites, and this is also confirmed by the crystallite sizes calculated from Rietvield refinement, listed in Table 4.1. A small increase in crystallite size from 4.4 nm for Ti-acidic to 4.7 nm for Ti-ref, and further to 6.0 nm for Ti-basic is observed.

The samples prepared with 10:1 molar ratio are phase pure anatase. In Figure 4.5 it can be observed that especially the (004) (middle peak of the three peaks around 38 °) peak is narrower than the other peaks, specially for the samples 10:1-ref and 10:1-basic. For 10:1-1min, 10:1-150 °C and 10:1-acidic little to no narrowing is observed. For 10:1-ref and 10:1-basic it is also possible to observe the separation of two of the three peaks in the triplet around 38°. This narrowing of the diffraction peak indicates larger crystallites, and this is also observed for the calculated crystallite size in Table 4.1, where 10:1-basic has the largest crystallites with 10.3 nm and 10:1-1min has the smallest with 3.7 nm. Rietvield refinement higligting the differences between 10:1-acidic and 10:1-basic is presented in Figure A.1 and A.2 respectively.

Samples prepared with 15:1 molar ratio behave the same as for 10:1 molar ratio, with the samples 15:1-basic and 15-ref showing a clear narrowing in the (004) peak.

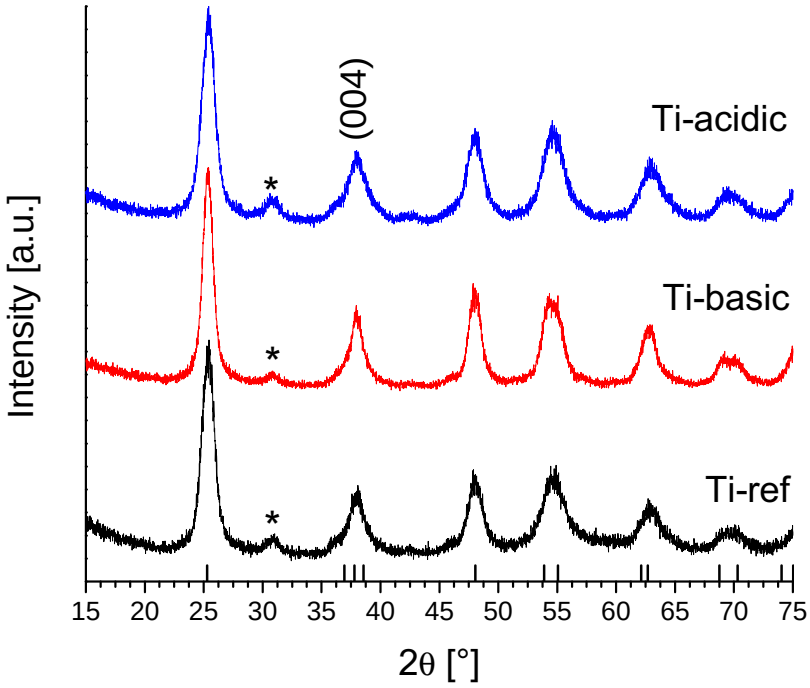

Figure 4.4: XRD patterns for unmodified TiO_2 nanoparticles. Diffraction lines for anatase from ICDD card #00-021-1272 are shown as bars, and the asterisk show diffraction line for the (121) peak of brookite from ICDD card #00-029-1360.

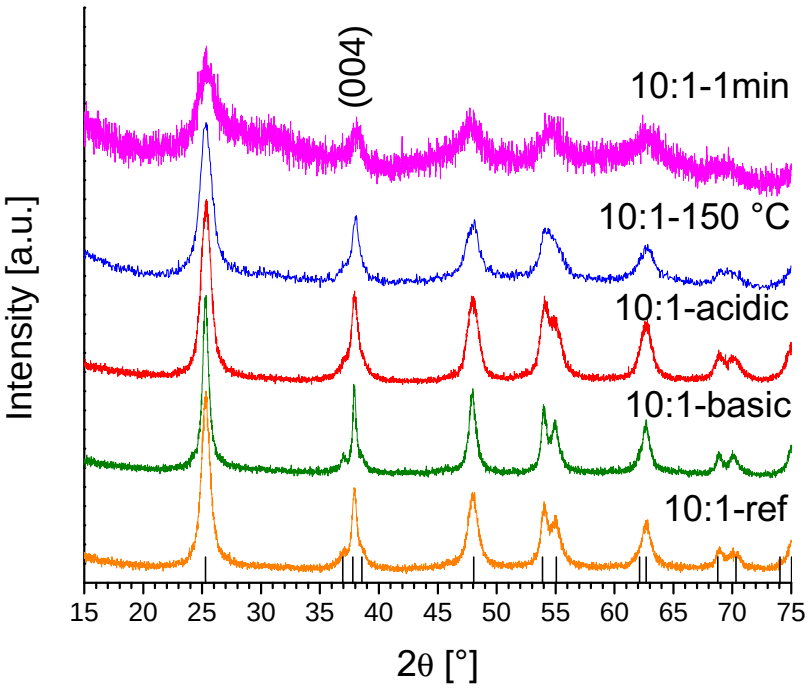

Figure 4.5: XRD patterns for *in situ* functionalized TiO_2 nanoparticles with 10:1 molar ratio. Diffraction lines for anatase from ICDD card #00-021-1272 are shown as bars.

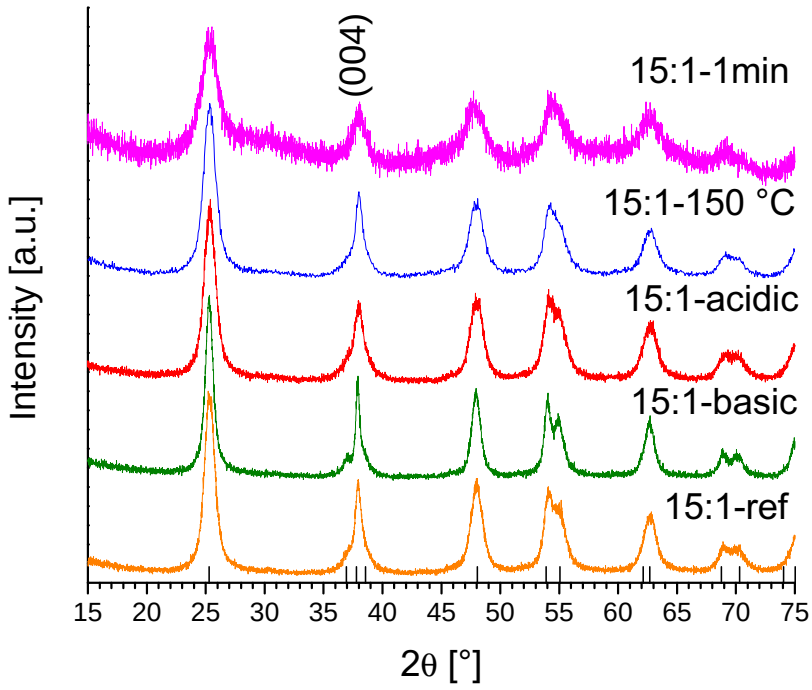

Figure 4.6: XRD patterns for *in situ* functionalized TiO_2 nanoparticles with 15:1 molar ratio. Diffraction lines for anatase from ICDD card #00-021-1272 are shown as bars.

4.1.3 Specific surface area and pores

Specific surface area from BET analysis

The nitrogen adsorption and desorption isotherms for unmodified and functionalized TiO_2 are presented to the left in Figure 4.7, 4.8 and 4.9 respectively. All the unmodified samples in Figure 4.7 show a clear hysteresis profile (splitting of the adsorption and desorption isotherm). A hysteresis profile is also present in all the samples with 10:1 and 15:1 molar ratio in Figure 4.8 and 4.9 respectively, but is not as prominent in all of them. As explained by Balbuena and Gubbins [44], a hysteresis profile is characteristic for mesoporous materials (pores with sizes ranging from 2 to 50 nm).

In Table 4.1 BET specific surface areas are presented, together with particle sizes calculated from BET specific surface area. The calculated particle sizes are also presented in Figure 4.10 together with particle size estimated from SEM images. Decreasing particle size (BET specific surface area increases) for decreasing reaction time and temperature compared to the reference samples are observed, showing similar trends as for particle size from SEM. Noteworthy in Figure 4.10 is that from SEM images 10:1-basic stands out with the largest particle size. From BET surface area the same sample shows a much smaller particle size compared to the rest of the samples, and actually smaller than both 10:1-ref and 10:1-acidic.

Pore size distribution from BJH analysis

The BJH desorption dV/dlog(D) pore volume is shown to the right in Figure 4.7, 4.8 and 4.9 for unmodified, 10:1 molar ratio and 15:1 molar ratio respectively. With the combination of non-porous particles observed from SEM, and a hysteresis profile as observed from nitrogen adsorption and desorption isotherms, the pore size distribution can be used as a measure of particle size as explained by Viana *et al.* [45]. In this work, pore size will then be used as a term for describing interparticle voids, and the average pore diameter will be directly correlated with particle size.

For all the unmodified samples a single narrow peak around 6 nm is observed in Figure 4.7. The average pore diameter is listed in Table 4.1 and only small differences is observed for the different reaction conditions. Also, good correlation between the average pore diameter and particle size from SEM and BET is seen.

For the functionalized samples a clear shift towards smaller pores is observed for decreasing reaction time and temperature compared to the reference samples, still having a narrow size distribution. The acidic samples have a similar size distribution as the reference sample, while the basic samples

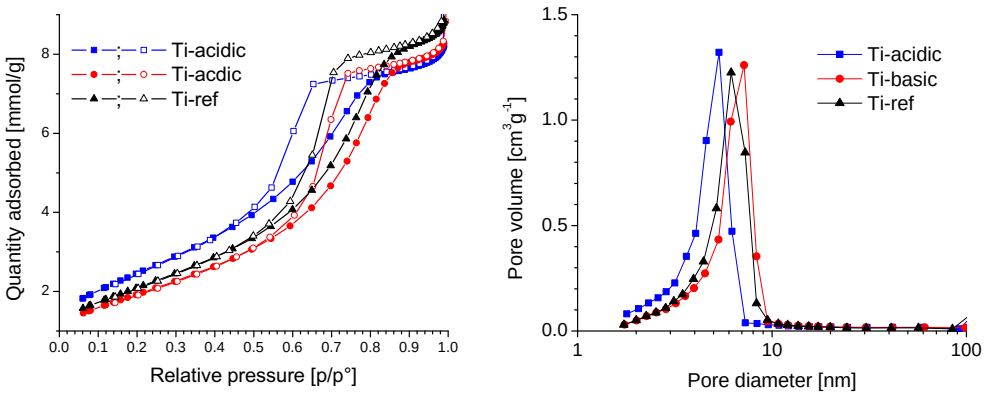

Figure 4.7: Nitrogen adsorption (solid symbols) and desorption (open symbols) isotherms (left), and BJH desorption dV/dlog(D) pore volume (right) for unmodified TiO_2 nanoparticles.

show a much broader size distribution. The average pore diameter for all functionalized samples are listed in Table 4.1.

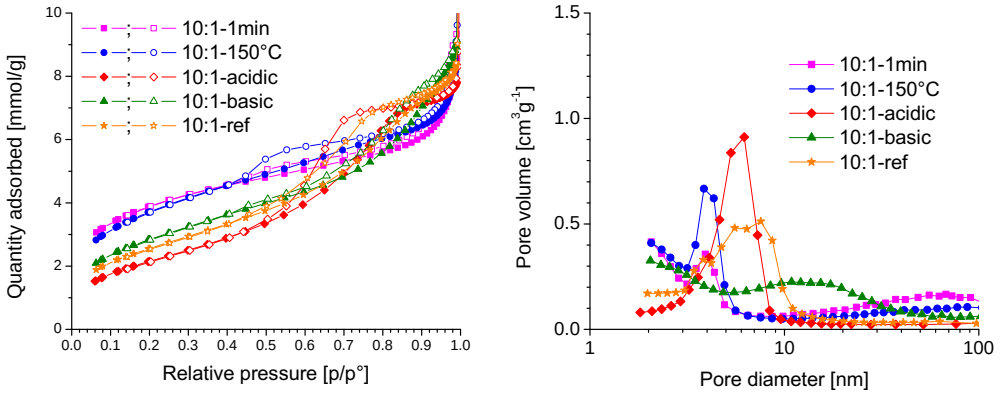

Figure 4.8: Nitrogen adsorption (solid symbols) and desorption (open symbols) isotherms (left), and BJH desorption dV/dlog(D) pore volume (right) for *in situ* functionalized TiO_2 nanoparticles with 10:1 molar ratio.

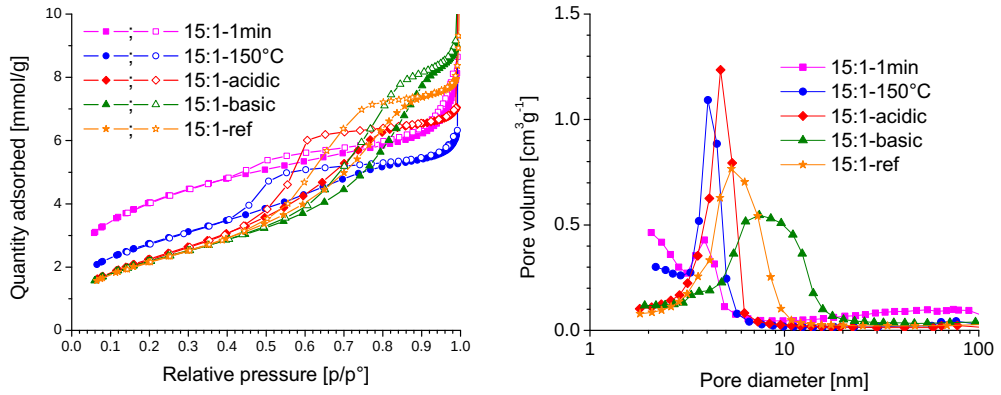

Figure 4.9: Nitrogen adsorption (solid symbols) and desorption (open symbols) isotherms (left), and BJH desorption dV/dlog(D) pore volume (right) for *in situ* functionalized TiO_2 nanoparticles with 15:1 molar ratio.

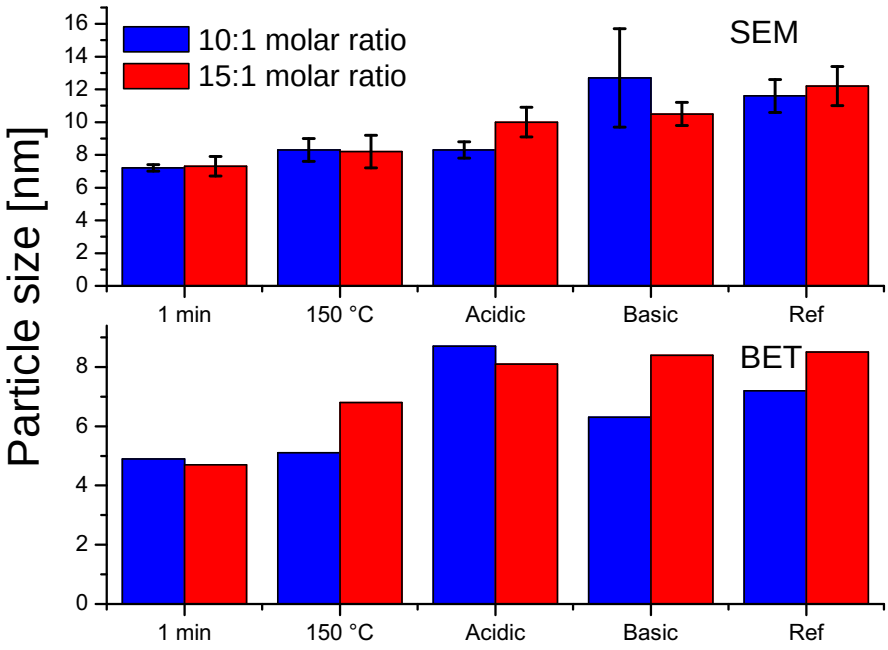

Figure 4.10: Particle size from SEM (top) and BET specific surface area (bottom) for functionalized TiO_2 nanoparticles.

4.1.4 Grafting of amino silane

In Figure 4.11, 4.12 and 4.13 mass loss as a function of temperature (left) and FTIR spectra (right) for unmodified and functionalized TiO_2 are presented. The TGA result for Ti-ref and 10:1-ref are reprinted from the work of Dalod *et al.* [7] to have the same heating procedure for all samples. All samples have been normalized relative to the mass of the sample right before the last heating step started (see Figure 3.2), for easier comparison. Under this normalization, a mass of 100 % would represent the mass of particles with amino silane, but without adsorbed water.

For the unmodified samples a small mass loss is observed from 150 to 400 °C, and this is assigned to hydroxyl groups on the surface that have not been successfully removed in the pretreatment steps. The presence of adsorbed water and hydroxyl groups is also confirmed by FTIR spectra. This is though at room temperature before heat treament. A clear difference is observed between Ti-basic and Ti-acidic, where Ti-acidic have a greater mass loss, and also more intense IR-bands assigned to water and hydroxyl groups.

All the functionalized samples show a greater mass loss in the range from 230 to 460 °C than unmodified TiO_2, and this mass loss is assigned to the combustion of organics, in this case APTES. The presence of amino silane on the particle surface is further confirmed by the FTIR spectra, all showing Ti-O-Si and N-H chemical bonds. All assignments of the observed adsorption bands are presented in Table 4.2. For the samples with 10:1 molar ratio, both 10:1-acidic and 10:1-ref stands out with a smaller mass loss than the rest. The samples with 15:1 molar ratio is believed to give a better picture of the true difference between the reference sample and the rest, since the reference sample here is not reprinted from the work of others. With respect to mass loss only, the acidic sample stands out with a significant lower mass loss, still having clear adsorption bands, when looking at the 15:1 molar ratio samples only.

The mass loss due to combustion of organics is listed in Table 4.1, together with the estimated surface coverage. Samples prepared with 15:1 molar ratio shows in general a smaller mass loss than 10:1 molar ratio. As no significant differences in mass loss is observed for other than the acidic sample, the differences in surface coverage is assigned to the differences in BET specific surface area.

In Figure B.1 and B.2 the FTIR spectra for the samples prepared for the authors specialization project is presented, and compared with unmodified TiO_2. All functionalized samples show the IR-bands presented in Table 4.2, indicating that chemical bonds have formed during synthesis.

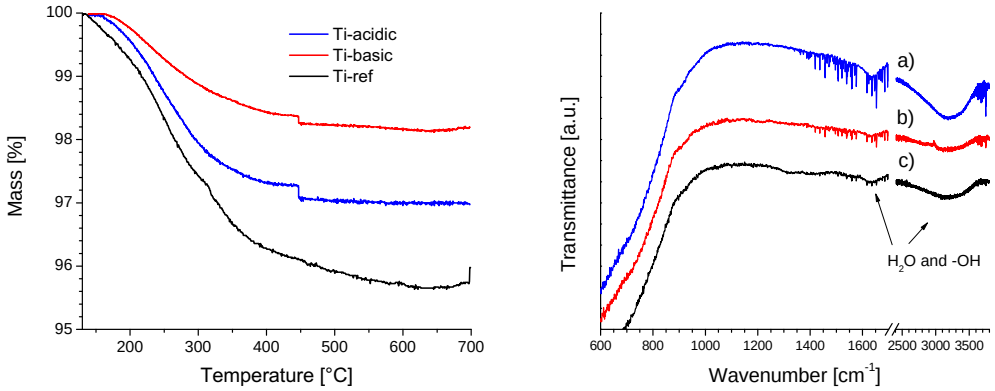

Figure 4.11: Relative mass loss as a function of temperature (left) and FTIR spectra (right) for unmodified TiO_2 nanoparticles.

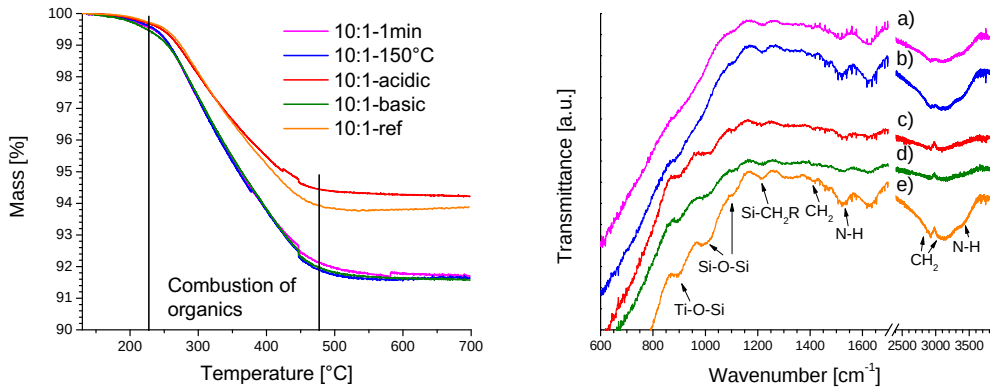

Figure 4.12: Relative mass loss as a function of temperature (left) and FTIR spectra (right) for *in situ* functionalized TiO_2 nanoparticles with 10:1 molar ratio. In the right figure the plots are labeled as follows: a) 10:1-1min, b) 10:1-150°C, c) 10:1-acidic, d) 10:1-basic, e) 10:1-ref.

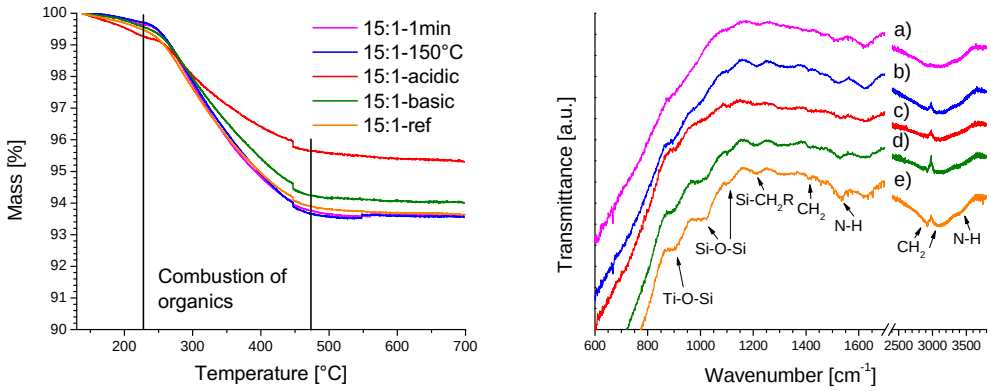

Figure 4.13: Relative mass loss as a function of temperature (left) and FTIR spectra (right) for *in situ* functionalized TiO_2 nanoparticles with 15:1 molar ratio. In the right figure the plots are labeled as follows: a) 15:1-1min, b) 15:1-150°C, c) 15:1-acidic, d) 15:1-basic, e) 15:1-ref.

Table 4.1: Properties of TiO_2 and *in situ* functionalized TiO_2 nanoparticles from XRD, SEM, TGA and N_2-adsorption. Standard deviation is only shown for particle size calculated from SEM pictures.

Sample	Crystallite size from XRD [nm]	Particle size from surface area [nm]	Particle size from SEM [nm]	Average pore diameter from BJH desorption [nm]	Specific surface area [m^2g^{-1}]	Organic mass loss [%]	Surface coverage [nm^{-2}]
10:1-1 min	3.7	4.9	7.2 ± 0.2	11.7	314	6.7	2.2
15:1-1 min	4.0	4.7	7.3 ± 0.6	9.1	328	5.4	1.7
10:1-150 °C	5.1	5.1	8.3 ± 0.7	6.5	304	7.0	2.4
15:1-150 °C	5.3	6.8	8.2 ± 1.0	12.2	226	5.6	2.6
10:1-Acidic	6.7	8.7	8.3 ± 0.5	14.6	177	5.0	2.9
15:1-Acidic	5.6	8.1	10 ± 0.9	6.6	190	3.4	1.9
10:1-Basic	10.3	6.3	13.7 ± 3.0	6.6	243	7.0	3.0
15:1-Basic	8.5	8.4	10.5 ± 0.7	8.0	183	5.1	2.9
Ti-Acidic	4.4	7.6	7.9 ± 0.6	7.3	203	N/A	N/A
Ti-Basic	6.0	9.7	9.1 ± 0.6	5.7	158	N/A	N/A
10:1-ref	7.3	7.2	11.6 ± 1	11.3	213	8.2	4
15:1-ref	6.3	8.5	12.2 ± 1.2	5.5	182	6	3.4
Ti-ref	4.7	9.0	9.3 ± 0.1	10.2	171	N/A	N/A

Table 4.2: Overview of characteristic IR-bands observed for TiO_2 and *in situ* functionalized TiO_2 nanoparticles.

Wavenumber	Assignment	Sample	Reference
<900	Ti-O-Ti	All samples	[6], [7]
900	Ti-O-Si	All functionalized samples	[7], [36], [37]
1020 and 1120	Si-O-Si	All functionalized samples	[6], [7], [37]
1220	Si-CH_2R	All functionalized samples	[7]
1460	CH_2 (deformation)	All functionalized samples	[7]
1530 and 3200-3500	N-H	All functionalized samples	[6], [7], [37]
1640 and 2500-3600	Adsorbed H_2O and -OH groups	All samples	[6], [7], [37]
2850 and 2920	CH_2 (stretching)	All functionalized samples	[6], [7], [36], [37]

4.2 Dispersion of TiO_2 nanoparticles

The results for the work on achieving a stable dispersion of TiO_2 nanoparticles is mostly based on the visual appearance of the dispersions. A stable dispersion of particles with primary particles around 10 nm (assuming no agglomerates) will appear transparent by visual inspection (assuming a transparent fluid), and will also have no sediments. For some investigations particle size distribution (PSD) was measured to see to what extent the method had an effect, if it had an effect at all.

In Figure 4.14 the size distribution is presented for Ti-ref, 10:1-15min (the most promising sample from the authors specialization project) and Ti-ref-stored (stored indicates that PSD results was obtained 6 months after synthesis). Knowing that the primary particle size is around 10 nm it is clear that the particle is very agglomerated, with agglomerate size ranging from 1 to 100 μm. From comparison of Ti-ref and Ti-ref-stored it can be seen that agglomeration probably happens during or right after the synthesis, since no significant change is observed as a function of ageing. It can also be observed that functionalizing with APTES does not hinder agglomeration in water, it actually leads to bigger agglomerates.

Figure 4.15 a) shows how 1.0 vol% of functionalized (10:1-15min) TiO_2 nanoparticles disperses in the polymer. The milky white colour indicates agglomerates. In the same figure the effect of one (b) and two (c) exposures of ultrasonification for 1 min at 30 % amplitude is shown. As can be seen, no visible effect is observed, and the particles are still agglomerated.

The result of dispersing 10:1-15min in diethyl ether is shown in Figure 4.16. The picture is taken after vigorous stirring, and clearly shows that a stable dispersion does not form, as the particles quite quickly sediments. The same result was obtained when using xylene as a solvent instead of diethyl

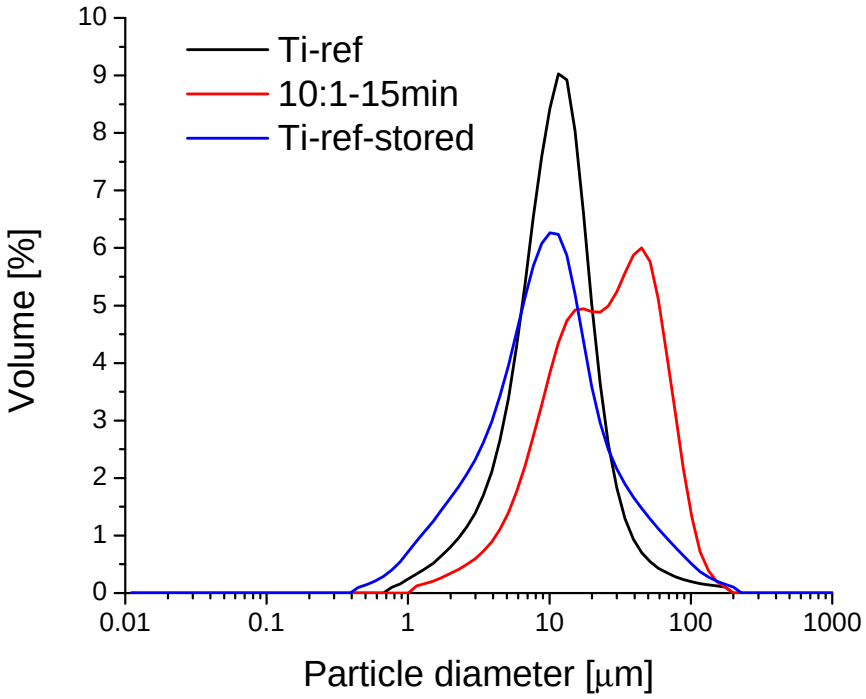

Figure 4.14: Particle size distribution of as synthesised Ti-ref (black line), 10:1-15min (red line) and Ti-ref about 6 months after synthesis (blue line).

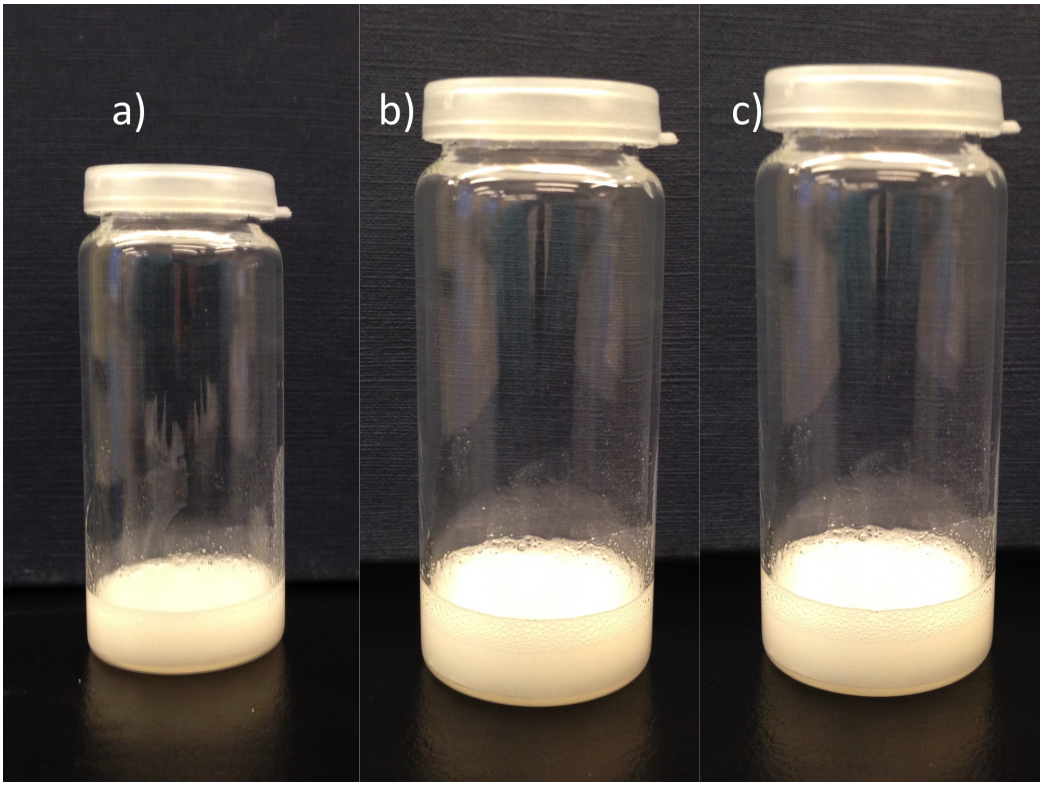

Figure 4.15: Funtionalized nanoparticles in the unpolymerised polymer before (a), and after first (b) and second (c) ultrasonfication for 1 min at 30 %.

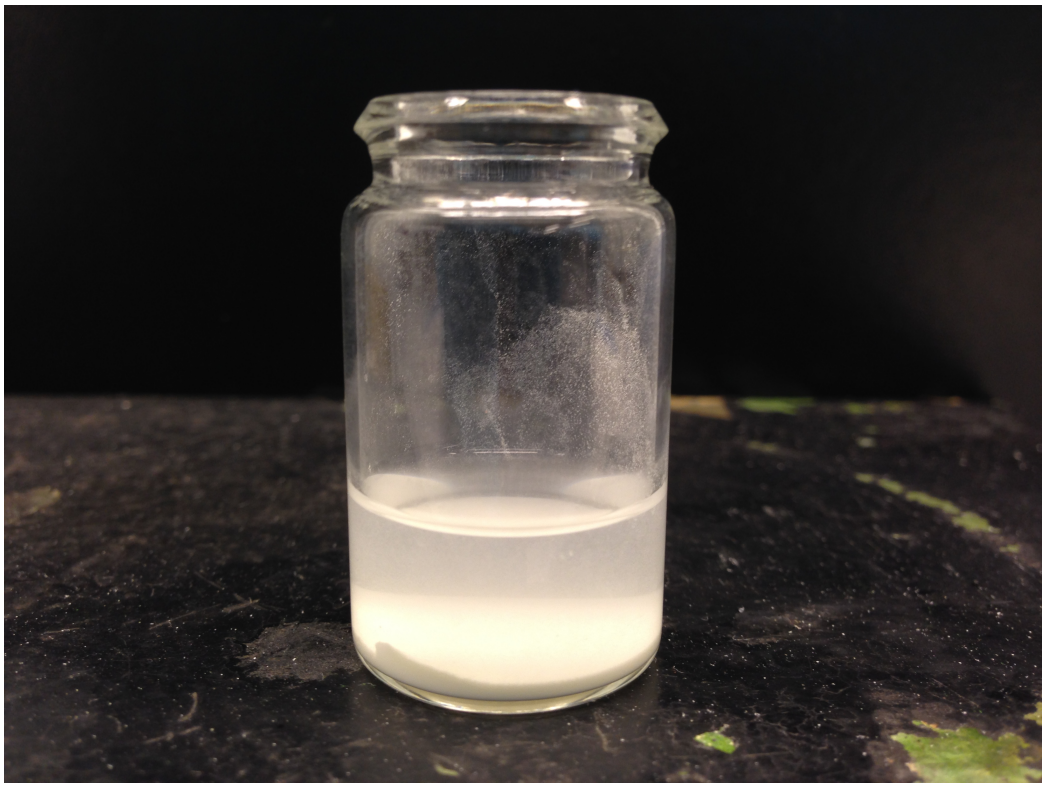

Figure 4.16: 10:1-15min mixed with diethyl ether showing sediments and large flocs.

ether. Further mixing with the polymer did not improve the dispersions, and the polymer-solvent-nanoparticle mixture showed a milky white colour for both solvents. Still, with the use of diethyl ether a polymer-nanoparticle composite (0.5vol%-10:1-15min) was made after evaporating away diethyl ether during continuous stirring.

The effect of longer exposures to ultrasonification was investigated for Ti-ref (1wt%) in water, and the results are presented in Figure 4.17. The right picture is taken as quickly as possible after ultrasonfification (10 min at 30 %), and sediments and flocs are clearly visible. The ultrasonification generated a lot of heat, and after cooling to room temperature a new exposure for 10 min at 50% amplitude was done with the same result, no visible change of the dispersion.

The effect of solid-liquid ratio on ultrasonfication was investigated, and the PSD results taken as quickly as possible after ultrasonification is presented in Figure 4.18, and the visible appearance of the samples before and after ultrasonification is presented in Figure 4.19. As can be seen, no signif-

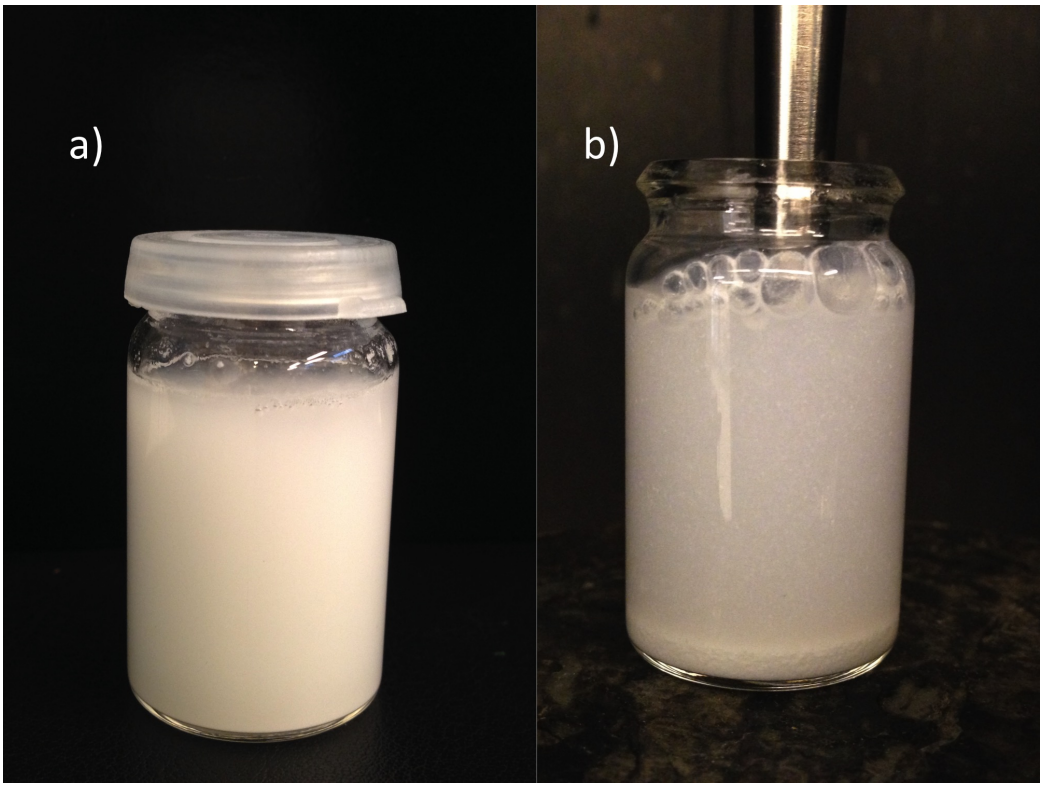

Figure 4.17: Ti-ref in water (a) and Ti-ref in water after 10 min at 30 % amplitude (b).

icant change in the particle size distribution, except for a peak appearing at 200 nm for the sample with 0.1 wt%. This peak disappears for 0.01 wt%, and 200 nm is also big for particles having a primary particle size of 10 nm. The visual appearance of the dispersion is also the same before and after ultrasonification.

The dispersions showed no visible effect of mixing with the surfactant SDS (was still milky white), except the fact that sedimentation happen much slower. No effect of ultrasonification before, after or before and after adding SDS was observed on the visible appearance of the dispersions.

For both unmodified and functionalized particles the same effect was observed when changing the pH of the aqueous dispersions. Sedimentation happened slower, indicating some degree of stabilization, but the dispersion was still milky white. This was the same as observed when adding SDS to a neutral aqueous dispersion of unmodified particles; slower sedimentation, but still a milky white colour.

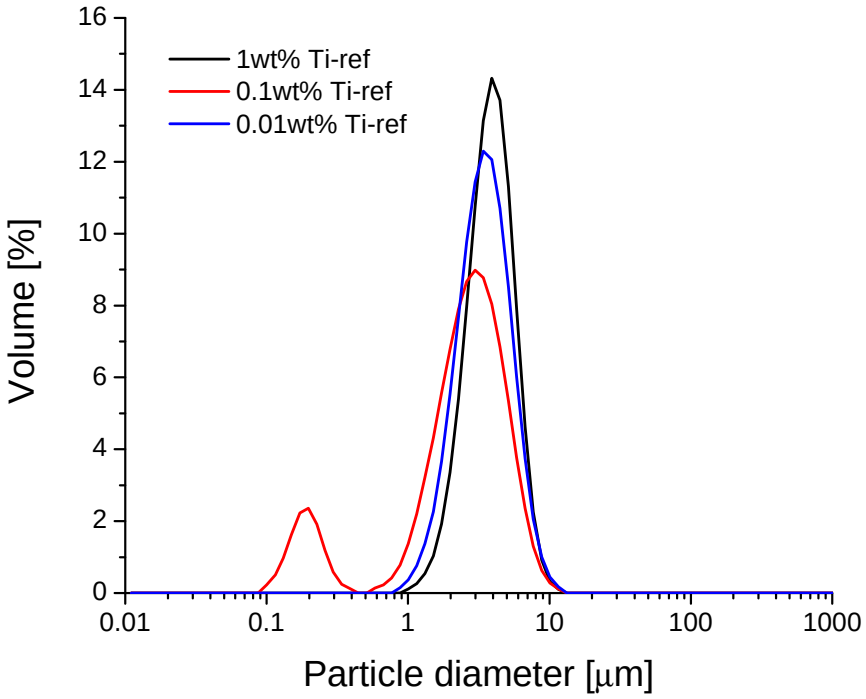

Figure 4.18: Particle size distribution showing the influence of solid-liquid ratio (TiO_2:water) on the effect of ultrasonification.

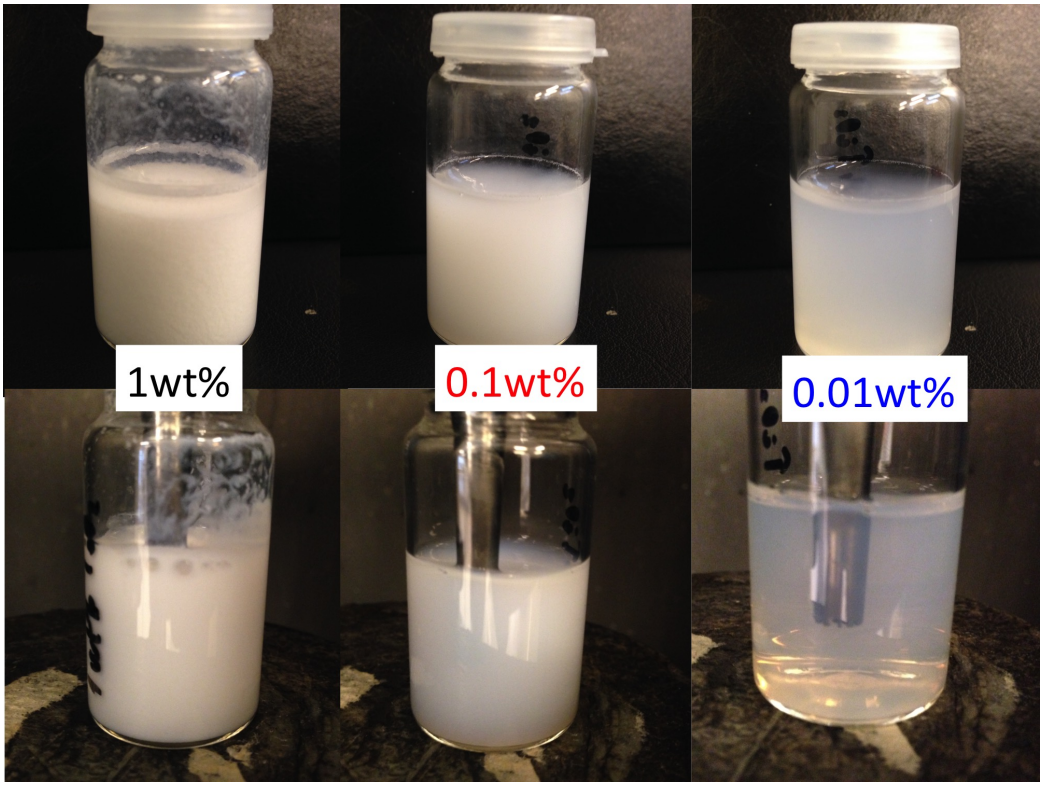

Figure 4.19: Picture before (top) and after (bottom) ultrasonification on dispersions containing 1, 0.1 and 0.01wt% unmodified TiO_2 nanoparticles in water.

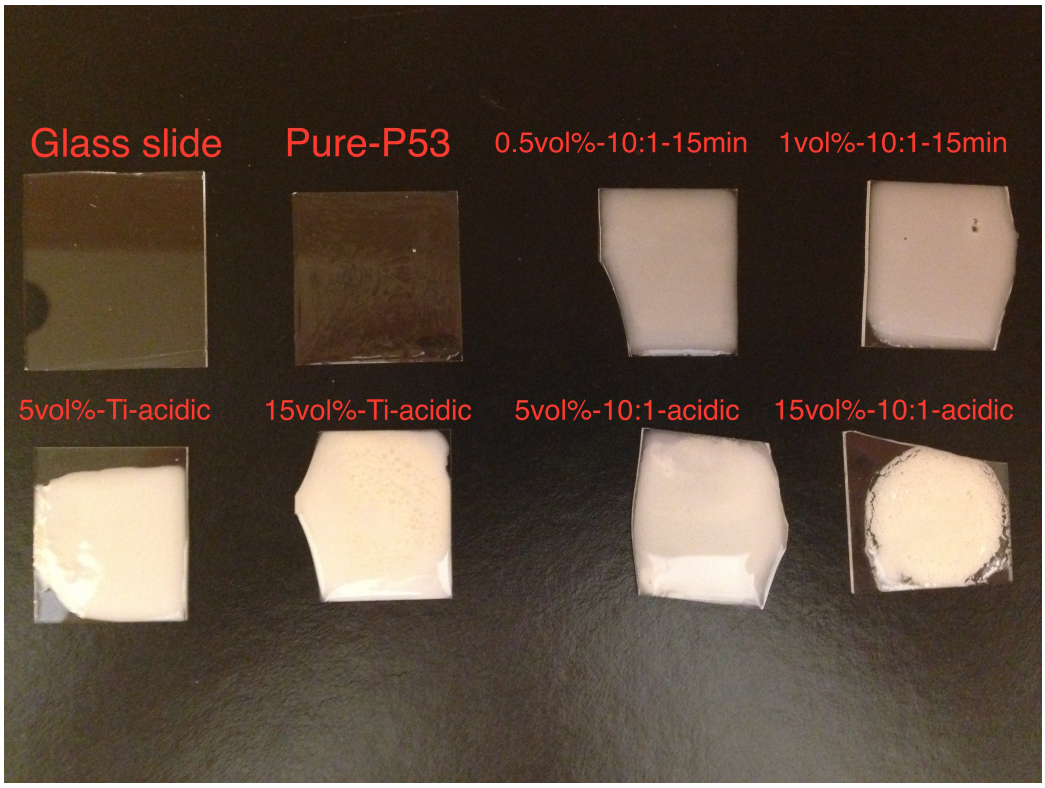

Figure 4.20: The visual appearance of all polymer-nanoparticle composites prepared, together with Pure-P53 and glass slide used as substrate for the films. All samples on the bottom did not polymerize.

4.3 Polymer-nanoparticle composite

Of the six polymer-nanoparticle composites that was prepared with particles, only two of them polymerized, namely 0.5vol%-10:1-15min and 1vol%-10:1-15min. The samples containing 5vol% particles had a visual appearance similar to those with 0.5 and 1vol%, see Figure 4.20, but were unpolymerized. In both samples with 15vol% it seems a phase separation has happened. From Figure 4.20 it can be seen that the particles are agglomerated, making the transparent polymer milky white. Only the polymerized samples were further characterized after synthesis.

4.3.1 Refractive index

The measured refractive index as a function of wavelength is presented in Figure 4.21. As no data fitting was possible, due to the thickness of the films, it is believed that the values must be understood as the value for the

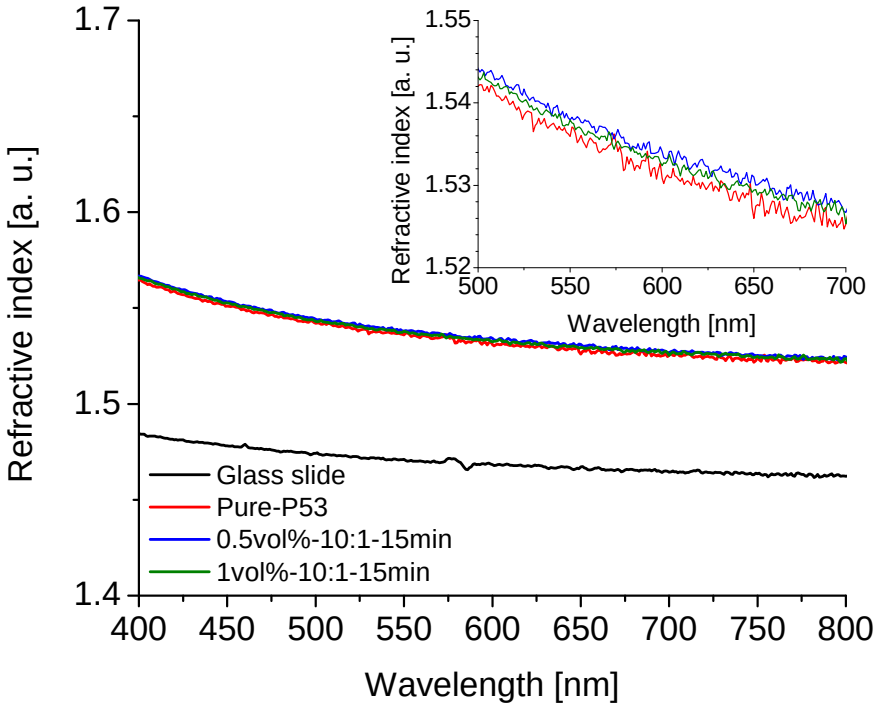

Figure 4.21: Refractive index for glass slide, Pure-P54 and the polymer-nanoparticle composites.

whole system (glass slide with polymer), and not the polymer film itself. The measured values for the glass slide and the polymer give very reasonable results knowing that the glass has a refractive index around 1.47 at 400 nm and 1.45 at 800 nm, and the polymer has a given value of 1.53. As can be seen from the inset a small increase in refractive index is observed for the films with particles, and the increase is in agreement with the linear relationship in Equation 4.1, especially for 0.5vol%. From this equation the theoretical values are 1.535 and 1.540 for 0.5 and 1vol% respectively. Noteworthy is that the refractive index for 1vol% is actually lower than for 0.5vol%, this is in disagreement with Equation 4.1.

$$n_{\text{Composite}} = n_{\text{Polymer}}\phi_{\text{Polymer}} + n_{\text{Particles}}\phi_{\text{Particles}} \tag{4.1}$$

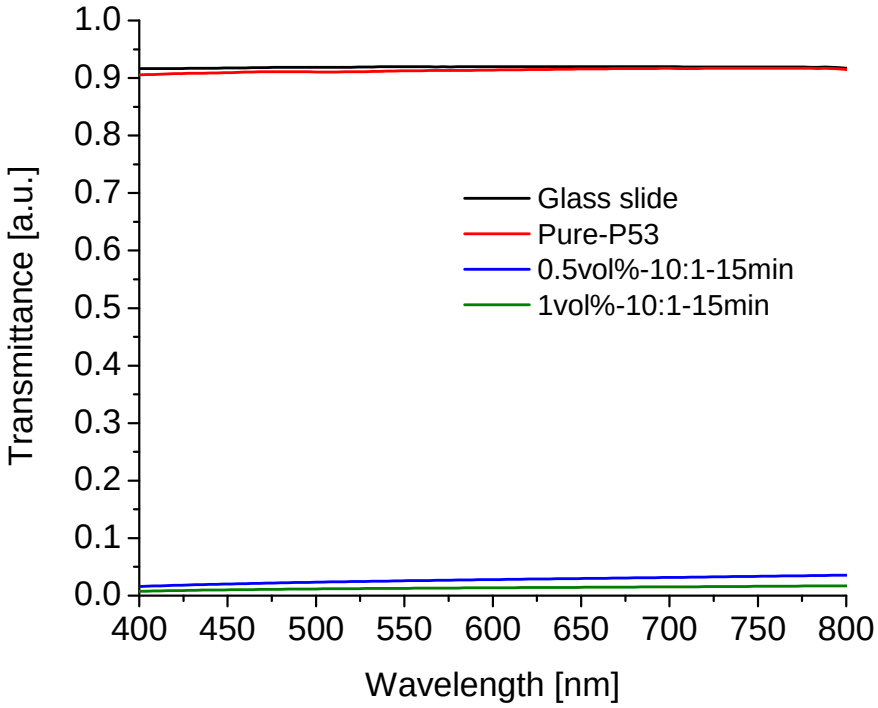

Figure 4.22: Transmittance for glass slide, Pure-P53 and the polymer-nanoparticle composites.

4.3.2 Transmittance

Measured transmittance is presented in Figure 4.22. It can be seen that the glass slide with and without the polymer almost have the same transmittance, indicating that the transmittance through the pure polymer is very close to 100 %. As expected from the visual appearance of the films with particles, the transmittance for these are close to 0 %. The film with 0.5vol% shows a slightly higher transmittance than the film with 1vol%, which is as expected.

4.3.3 E-modulus

The E-modulus for the polymers was tried to measured by QNM mapping with an AFM. As seen in Figure 4.23 this was very challenging, as the AFM tip and cantilever became embedded in the polymer, making measurements impossible. Figure 4.23 shows to the left how the tip (SNL-10, pointing down) and the cantilever drastically deforms the polymer, while in the right

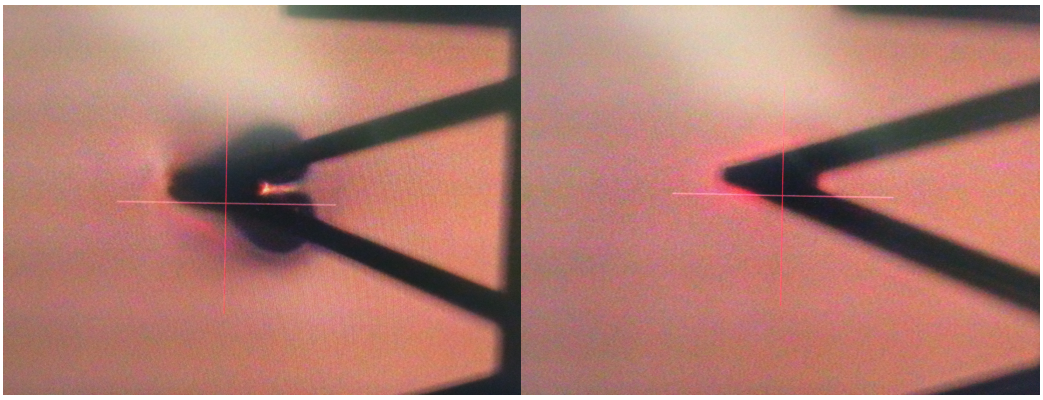

Figure 4.23: Image showing how the AFM-tip (facing downwards) and cantilever drastically deformed the sample (left), and AFM-tip (facing downwards) and cantilever after separation from the sample (right).

picture it shows the undeformed polymer after the polymer has released the tip/cantiliver. With an optical microscope focused on the tip and sample surface, it was possible to see how the cantilever sprung back to position after the polymer let go of the tip. By inspection of the AFM-tip after it was used, it was possible to see that the cantilever had been bent from the interaction with the polymer. A tip with a larger tip radius (MLCT) was then tested, in hope that it would not penetrate the surface of the polymer to the same degree, and therefore avoid the problem with the high adhesion forces. The results was the same as for the tip with a smaller tip radius. This made it so that no measurements was done on P53.

In Figure 4.24 a mapping of the E-modulus of polydimethylsiloxane (PDSM) obtained by the same method as tried for P53 is shown. From this an average value of around 1.2 MPa was obtained, which is a very reasonable value for PDMS. This shows that the method used gives reasonable results under correct operation with a suitable tip (tip radius, cantilever stiffness, tip material). The combination of a very soft and sticky polymer made finding the correct tip and operation conditions too big a challenge for this work.

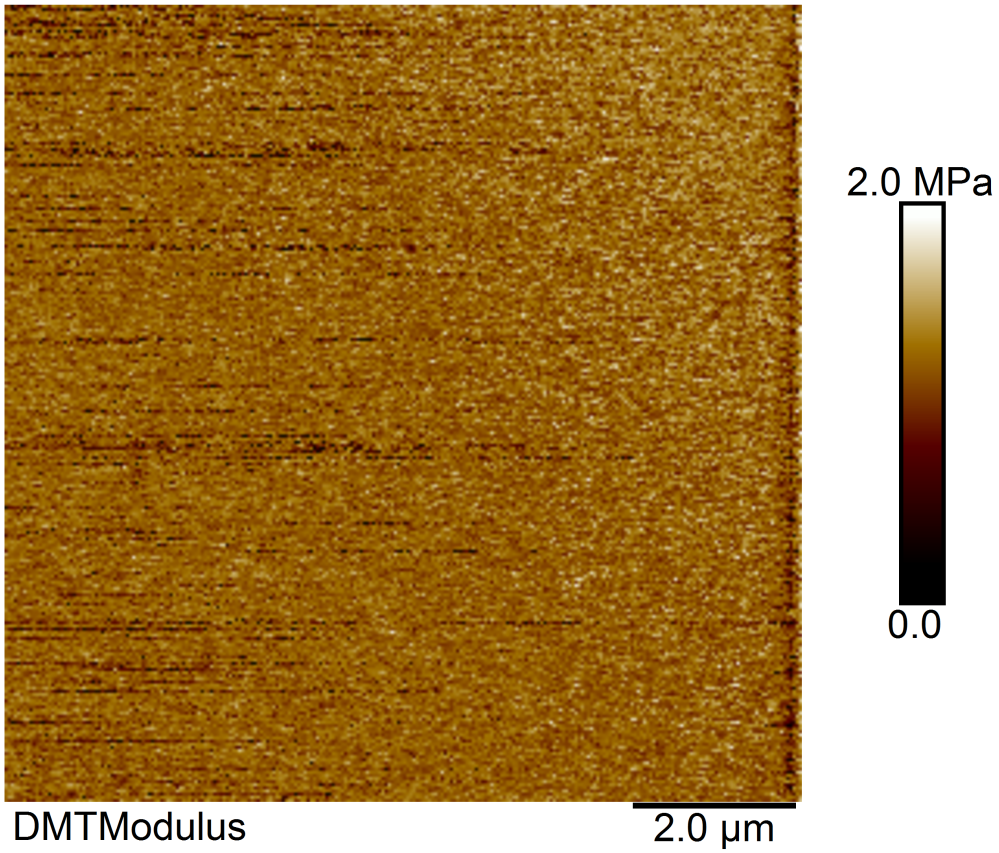

Figure 4.24: E-modulus measured with AFM QNM on a PDSM sample. Average value was estimated to 1.2 MPa. Retrieved from [46].

Chapter 5

Discussion

5.1 TiO_2 nanoparticles

From SEM pictures and TGA combined with FTIR, it is clear that *in situ* functionalized TiO_2 nanoparticles have been successfully made from a hydrothermal synthesis route.

5.1.1 Particle size and morphology

From the SEM pictures of unmodified TiO_2 nanoparticles (Figure 4.1) a small increase in particle size is observed when going from acidic to basic reaction conditions. This indicates that the pH have little to no influence on the formation of TiO_2 nanoparticles from a TIP precursor mixed with water. This is the same results reported by Barbé *et al.* [31]. Barbé *et al.* explanation is that Ostwald ripening is promoted under basic reaction conditions, leading to slightly larger particles.

For the functionalized samples prepared with 10:1 and 15:1 molar ratio it is observed that 1 min reaction time gives smaller and fewer elongated particles compared to the reference sample (120 min reaction time). This follows the trend observed in the authors specialization project, where a clear decrease in particle size was observed when reducing the reaction time from 120 to 15 min. Oriented attachment is reported to be the main reason for the formation of the elongated particles, both in the work by Dalod *et al.* and Penn and Banfield [33]. Dalod *et al.* also suggested that specific adsorption of APTES would guide the growth, which would further promote oriented attachment. As oriented attachment must be a time consuming reaction, it is reasonable that shorter reaction time will give fewer elongated particles. Lowering the reaction temperature also gives smaller particles observed from the SEM pictures. This is reasonable, as reducing the temperature effectively

also reduces the reaction time, as the heating and cooling will be faster. Both the effects seen from time and temperature is consistent with what Hayashi and Torii [30] and Horvat *et al.* [34] have reported for pure TiO_2.

By changing the pH of the reaction media, a big change in morphology and particle size is observed for the functionalized samples (Figure 4.2 and 4.3). It is clear that the formation of elongated particles is promoted under basic conditions with the presence of APTES. One possible explanation for this is that the acidic condition catalyses the condensation reaction between TiO_2 and APTES, capping the particles quicker, and thus leaving shorter time for oriented attachment to happen. As both 10:1-acidic and 15:1-acidic stands out with a smaller weight loss from TGA, it is not likely that this is the correct explanation, since this at least should have lead to the same mass loss as for the other samples. Another explanation could be that the acidic environment alter the surface groups on the TiO_2 in such a way that there is no specific adsorption of APTES, leading to less anisotropic growth, and further suppressing the formation of elongated particles. In the work done by Penn and Banfield [33], HCl (aq) was shown to lead to less anisotropic growth for unmodified TiO_2 nanoparticles. This could also be a possible mechanism happening with nitric acid. As always, it is difficult to know exactly what is happening inside the autoclave, and little to no work has been done on this system earlier (TIP, APTES and acidic or basic conditions), but it is clear that it is the combination of APTES and basic conditions that promotes the formation of elongated particles.

5.1.2 Phase purity, composition and crystallinity

All the unmodified samples are nanocrystalline, and mainly anatase, but with significant amounts of brookite. For Ti-ref both the crystallite size and amount of brookite is consistent with what has been reported earlier, by Dalod *et al.* [7] and Barbé *et al.* [31].

The *in situ* functionalized samples are nanocrystalline and purely anatase. This is exactly the same results as reported by Dalod *et al.* [7] and seen in the authors spesalization project [8]. The most prominent future from the XRD plots is the narrowing of the (004) peak for functionalized samples compared with Ti-ref. This is especially visible for 10:1-basic. The narrowing of the (004) peak indicates and increase in crystallite size in the [001] direction (gives more (004) planes that will give a narrower diffraction peak). This, in combination with the elongated particles observed in the SEM pictures, makes it clear that the elongation of the particles has happened along the [001] direction. This is also confirmed by investigation in high resolution transmission electron microscopy (HRTEM) in the work Dalod *et al.* [7], as

shown in Figure 5.1. This strengthens the theory about oriented attachment being one mechanism for formation of the elongated particles observed in SEM pictures.

5.1.3 Specific surface area and pores

For all the unmodified samples the particle size calculated from BET surface area are in the same range as the estimated particle size from the respective SEM images. This indicates a dried powder with little surface interaction between the particles (most of the particle surface is accessible to nitrogen adsorption), which in turn should indicate a weakly agglomerated powder. The same is seen for the samples prepared with APTES. The BET surface area show the same trends as the particle size estimated from SEM images show, except for 10:1-basic. 10:1-basic shows a significant higher BET surface area, giving a considerable smaller particle size than expected from SEM images. The nitrogen adsorption for this sample was re-done to assure that the measurement was not just an abnormally experiment. The increase in BET surface area can be explained by the fact that hydrolysis of APTES is promoted under basic conditions, so that small clusters (only a few atoms) of SiO_2 may be formed, and that these small clusters give rise to an unreasonable high specific surface area. The reason it is not detected in the SEM is because they would be very small, and the amount would be so small that detection by XRD or FTIR would not be possible.

As the pore size is expected to correlate with the particle size because of the hysteresis profile seen in all samples, it is expected to see the same trends for the pore size distribution as for particle size from SEM images and BET surface area. For the unmodified samples just small shifts in the peak positions are seen in Figure 4.7, which is consistent with the observation from SEM and BET. Consistency with SEM and BET is also seen for the functionalized samples, where the samples A-1 min, A-150 °C and A-acidic are slightly shifted towards smaller pore sizes compared with the reference samples. The two samples with basic reaction conditions show a broader pore size distribution which is also shifted towards higher pore sizes. This is consistent with seeing a mix of big elongated particles together with small spherical particles in the SEM images. The same trends are also seen for the average pore diameter from BJH desorption.

5.1.4 Grafting of amino silanes

In the TGA plots in Figure 4.12 and 4.13 the samples 10:1-acidic and 15:1-acidic stand out from the rest with significantly smaller weight loss. This is

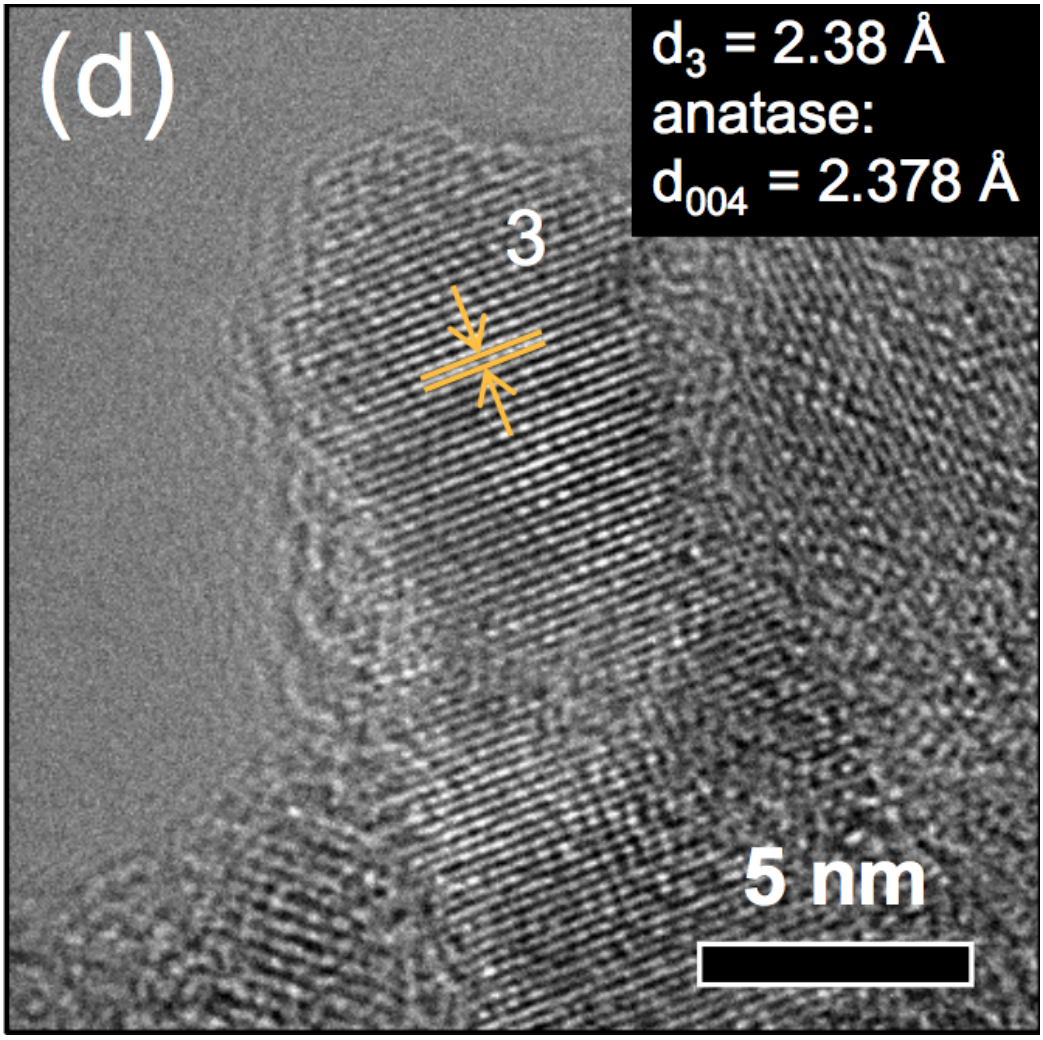

Figure 5.1: HRTEM image of elongated TiO_2 particle showing elongation along the [001] direction. The synthesis parameters used for this sample is the same as for 10:1-ref. Retrieved from [7].

probably because acidic conditions act as an inhibitor on the condensation reaction between APTES and TiO_2. The mass loss of this sample is still greater than that of unmodified TiO_2 in the temperature interval for combustion of organics, indicating grafted APTES. The grafted APTES is also confirmed by FTIR spectroscopy, where especially the presence of Ti-O-Si and N-H chemical bond indicates that APTES is grafted to the surface of TiO_2. A successful grafting of APTES is seen for all reaction conditions.

The mass losses and the estimated surface coverage is comparable to what have been reported by Dalod *et al.* [7] and Zhao *et al.* [6]. An estimated surface coverage around 2 molecules/nm^{-1} is considered a good surface coverage. With respect to the difference between 10:1 and 15:1 molar ratio, 15:1 molar ratio always has a smaller mass loss than the respective 10:1 molar ratio sample. This is as expected, since less APTES is added, and from Le Châtelier's principle the consumption of APTES should then be less.

5.2 Dispersion of TiO_2 nanoparticles

From the PSD results and visual appearance of the dispersions prepared it is clear that the TiO_2 nanoparticles are agglomerated from the synthesis, both for unmodified and functionalized particles. For unmodified samples this is in agreement with what reported by Barbé *et al.* [31]. A possible solution for achieving non-agglomerated particles from synthesis is to utilize a very acidic reaction envirmoent, as done by Chae *et al.* [32]. They report that close to non-agglomerated particle with a primary particle size of 7 nm was achieved using a mixture of water and ethanol with pH at 0.7. This will on the other hand ruin some of the "greenes" of the hydrothermal synthesis. The *in situ* functionalization was not successful in avoiding agglomeration.

None of the approaches used for preparation of a stable dispersion resulted in a sufficient de-agglomeration (reducing the agglomerates down to 10 nm) effect. This is consistent with what found from literature, where only one highly specialized attrition bead mill [23] have been found to report the successful de-agglomeration down to particle sizes close to 10 nm. Interesting to observe is that the functionalized particles seem to behave similarly in water as in the used organic solvents. This can be explained by the fact that the tail of APTES with an amino group at the end it not fully polar or non-polar, but is somewhere in between. This can result in poor dispersibility in the polar solvent water and non-polar organic solvents. Better results may have been achieved by a mixed solvent, or a different functionalizing agent.

Electrostatic stabilization with changing pH and stabilization with SDS resulted in longer sedimentations time, but no de-agglomeration. In the

work by Imae *et al.* [5] and Yang *et al.* [4] the effect of pH and SDS is investigated respectively. They both report increased stabilization, but they do no investigation of the size of the stabilized particles or agglomerates. The results from this work show that SDS and pH have a stabilizing effect as expected from theory (Section 2.2.3) and literature, but little to no effect on the de-agglomeration of the particles synthesized in this work.

5.3 Polymer-nanoparticle composite

Even though primary particles in a stable dispersion was not achieved, polymer-nanoparticle composites was prepared with the agglomerated particles. The polymer-nanoparticle was successfully prepared with 0.5 and 1vol% particles, but the polymerization process was effectively stopped by addition of 5 and 15vol% particles. This was difficult to improve, since knowledge about the polymer and polymerization process is only held by the people at poLight AS. Both methods used for preparation of the polymer-nanoparticle composite will be applicable when a stable dispersion of primary particles is achieved.

5.3.1 Refractive index

The refractive index measured for the glass slide and the Pure-P53 are both close to what was expected, so even though a modelling of the measured results was not possible, it seems like the results at least can be used for relative comparison. The increase in refractive index observed for 0.5vol%-10:1-15min relative to Pure-P53 is as expected. The fact that 1vol%-10:1-15min does not show a higher refractive index than 0.5vol%-10:1-15min is difficult to explain. As a phase separation was observed for higer particle concentrations, it could be that some degree of phase separation has happen for 1vol%-10:1-15min as well, leading to the lower refractive index. It could also be that the differences observed are not due to the particles, but is actually the inaccuracy induced in the measurements by not being able to fit the data.

5.3.2 Transmittance

As agglomerated particles with a size around 10 μm was dispersed in the polymer, the very low transmittance is as expected from the theory and equations in Subsection 2.1.2. By dispersion of non-agglomerated particles with a size of 10 nm it is expected that the transmittance will increase. On

the other hand, Pure-P53 have a transmittance close to 100%, making it highly suitable for applications like lenses.

5.3.3 E-modulus

The E-modulus ended up being too challenging to measure as a part of this work. Proof of concept was shown by Dalod [46] when measuring the E-modulus of a PDMS sample to be around 1.2 MPa. The adhesion between the sample and AFM tip seemed to be the major problem when measuring on P53. Thus by coating or functionalizing the AFM-tip with a material or molecule that lowers the adhesion, it may be possible to use this approach to measure the E-moduls of P53 and the polymer-nanoparticle composites as well.

Chapter 6

Concluding remarks and further work

A polymer-nanoparticle composite for use as a lens has been made by dispersing *in situ* functionalized TiO_2 nanoparticles into the polymer named P53, for the purpose of increasing the refractive index of the polymer. Investigation of the composites optical properties has been performed, while investigation of mechanical properties was unsuccessful. Since the TiO_2 nanoparticles was agglomerated, and any approach used for de-agglomerating them was unsuccessful, the transmittance of visible light through the polymer was severely impaired with the introduction of particles. An increase in refractive index was observed with the introduction of particles. It was also found that with a particle content of 5vol% or higher in the polymer, the polymerization process was stopped.

To achieve a polymer-nanoparticle composite useable for use in poLight AS TLens®, work on achieving a stable dispersion of non-agglomerated particles must be done if this method is to be used. Also, the issue with particles stopping the polymerization process must be overcome.

In addition, a further investigation of the mechanisms for the formation of elongated particles under hydrothermal synthesis used for making the *in situ* TiO_2 nanoparticles was done. The effect of further decreasing the reaction time from what was done in the authors specialization project [8] was studied. The effect follows the same trend as reported there, where shorter reaction time gave smaller particles and fewer elongated particles. Reducing the reaction temperature had the same effect as reducing reaction time, probably because the effective reaction time is also reduced by reducing reaction temperature. Most interesting was the big change between acidic and basic reaction conditions on the morphology of *in situ* functionalized particles, compared to the small effect this had on the unmodified particles. This

will be further investigated at the synchrotron facilities at the European Synchrotron Radiation Facility (ESRF) by Antoine Dalod, the co-supervisor of this work. It is believed to be a combination of oriented attachment and selective adsorption of functionalizing agent on different crystallographic faces that governs the formation of the elongated particles.

As good control over the morphology of the synthesized particles is now achieved, a further improvement of this synthesis route must be to achieve non-agglomerated particles. This seems difficult to achieve, but by very acidic conditions this could be possible. Then a synthesis route for *in situ* functionalized non-agglomerated TiO_2 nanoparticles with a particle size around 10 nm would have been developed, but as seen from TGA, this would lead to reduced grafting efficiency.

Bibliography

[1] Press release on poLight AS and BARTEC PIXAVI AS collaboration. http://vikingventure.com/wp-content/uploads/2015/03/PoLight_demonstrates_TLensTouchRefocusphone.03.02.2015.pdf, March 2015.

[2] poLight. TLens info. http://www.polight.com/key-advantages-10.html, September 2015.

[3] E. Ritzhaupt-Kleissl, J. Boehm, J. Hausselt, and T. Hanemann. Thermoplastic polymer nanocomposites for applications in optical devices. *Materials Science and Engineering: C*, 26(5–7):1067 – 1071, 2006.

[4] Yung-Jih Yang, Aniruddha V. Kelkar, Xilan Zhu, Guanrong Bai, Hou T. Ng, David S. Corti, and Elias I. Franses. Effect of sodium dodecylsulfate monomers and micelles on the stability of aqueous dispersions of titanium dioxide pigment nanoparticles against agglomeration and sedimentation. *Journal of Colloid and Interface Science*, 450:434 – 445, 2015.

[5] T. Imae, K. Muto, and S. Ikeda. The pH dependence of dispersion of TiO_2 particles in aqueous surfactant solutions. *Colloid and Polymer Science*, 269(1):43–48, 1991.

[6] Jie Zhao, Maria Milanova, Marijn M.C.G. Warmoeskerken, and Victoria Dutschk. Surface modification of TiO_2 nanoparticles with silane coupling agents. *Colloids and Surfaces A: Physicochemical and Engineering Aspects*, 413:273 – 279, 2012. 25th Meeting of the European Colloid and Interface Society25th Meeting of the European Colloid and Interface Society.

[7] Antoine R. M. Dalod, Lars Henriksen, Tor Grande, and Mari-Ann Einarsrud. Functionalized TiO_2 nanoparticles by single-step hydrothermal synthesis: the role of the silane coupling agents. In review, 2016.

[8] O. G. Grendal. "Hydrothemal syntehsis of *in situ* functionalized TiO_2 nanoparticles with amino silane", Dec. 2015. Specialization project.

[9] Linda S. Schadler. *Nanocomposite Science and Thecnology*, chapter 2, pages 77–153. Wiley-VCH Verlag GmbH and Co. KGaA, 2004.

[10] Changli Lu and Bai Yang. High refractive index organic-inorganic nanocomposites: design, synthesis and application. *J. Mater. Chem.*, 19:2884–2901, 2009.

[11] L. Zimmermann, M. Weibel, W. Caseri, U. W. Suter, and P. Walther. Polymer nanocomposites with "ultralow" refractive index. *Polymer Advanced Tecnhnologies*, 4(1):1–7, January 1993.

[12] Tao Li, Quan Chen, Linda S. Schadler, Richard W. Siegel, John Mendel, and Glen C. Irvin. Scratch behavior of nanoparticle Al_2O_3-filled gelatin films. *Polymer Composites*, 23(6):1076–1086, 2002.

[13] Norio Taniguchi. On the basics concept of nano-technology. In *Proceedings of the Iternational Conference on Production Enginering, Tokyo, 1974, Part II*, 1974.

[14] National Nanotechnology Initiative strategic plan, Desember 2004.

[15] Claudia Altavialla and Enrico Ciliberto, editors. *Inorganinc Nanoparticles Synthesis, Applications and Perspectives*. CRC Press, 2011.

[16] Celso de Mello Donegá, editor. *Nanoparticles Workhorses of nanoscience*. Springer, 2014.

[17] Hengzhong Zhang and Jillian F. Banfield. Structural characteristics and mechanical and thermodynamic properties of nanocrystalline TiO_2. *Chemical Reviews*, 114(19):9613–9644, 2014.

[18] Pavan K. Naicker, Peter T. Cummings, Hengzhong Zhang, and Jillian F. Banfield. Characterization of titanium dioxide nanoparticles using molecular dynamics simulations. *The Journal of Physical Chemistry B*, 109(32):15243–15249, 2005. PMID: 16852930.

[19] Mari-Ann Einarsrud and Tor Grande. 1D oxide nanostructures from chemical solutions. *Chem. Soc. Rev.*, 43:2187–2199, 2014.

[20] Parr Instrument Company. *Autoclave operating intructions, 4744-49 Acid Digestion Vessels*.

[21] C. Sauter, M.A. Emin, H.P. Schuchmann, and S. Tavman. Influence of hydrostatic pressure and sound amplitude on the ultrasound induced dispersion and de-agglomeration of nanoparticles. *Ultrasonics Sonochemistry*, 15(4):517 – 523, 2008.

[22] David W. Richerson. *Modern ceramic engineering: properties, processing, and use in design*, volume Third Edition. CRC Press, 2006.

[23] Mitsugi Inkyo, Takashi Tahara, Toru Iwaki, Ferry Iskandar, Christopher J. Hogan Jr., and Kikuo Okuyama. Experimental investigation of nanoparticle dispersion by beads milling with centrifugal bead separation. *Journal of Colloid and Interface Science*, 304(2):535 – 540, 2006.

[24] Prakash Khadka, Jieun Ro, Hyengmin Kim, Iksoo Kim, Jeong Tae Kim, Hyunil Kim, Jae Min Cho, Gyiae Yun, and Jaehwi Lee. Pharmaceutical particle technologies: An approach to improve drug solubility, dissolution and biovailability. *Asian Journal of Pharmaceutical Science*, 9(6), June 2014.

[25] `http://www.civilengineeringhandbook.tk/powder-metallurgy/attrition-mills.html`, June 2016.

[26] Philippe Sciau. Nanoparticles in ancient materials: The metallic lustre decorations of medieval ceramics. In Dr. Abbass A. Hashim, editor, *The deliver of nanoparticles*, chapter 25, pages 525–541. InTech, 2012.

[27] Akane Okada, Yoshiaki Fukushima, Masaya Kawasumi, Shinji Inagaki, Arimitsu Usuki, Shigetoshi Sugiyama, Toshio Kurauchi, and Osami Kamigaito. "Composite material and process for manufacturing same". U. S. Patent: 4,739,007, April 19, 1988.

[28] Sarita Kango, Susheel Kalia, Annamaria Celli, James Njuguna, Youssef Habibi, and Rajesh Kumar. Surface modification of inorganic nanoparticles for development of organic–inorganic nanocomposites—a review. *Progress in Polymer Science*, 38(8):1232 – 1261, 2013. Topical Issue on Polymer Hybrids.

[29] Jinghuan Zhang, Xin Xiao, and Junmin Nan. Hydrothermal-hydrolysis synthesis and photocatalytic properties of nano-TiO_2 with an adjustable crystalline structure. *Journal of Hazardous Materials*, 176(1–3):617 – 622, 2010.

[30] Hiromichi Hayashi and Kazuo Torii. Hydrothermal synthesis of titania photocatalyst under subcritical and supercritical water conditions. *J. Mater. Chem.*, 12:3671–3676, 2002.

[31] Christophe J. Barbé, Francine Arendse, Pascal Comte, Marie Jirousek, Frank Lenzmann, Valery Shklover, and Michael Grätzel. Nanocrystalline titanium oxide electrodes for photovoltaic applications. *Journal of the American Ceramic Society*, 80(12):3157–3171, 1997.

[32] Seung Yong Chae, Myun Kyu Park, Sang Kyung Lee, Taek Young Kim, Sang Kyu Kim, and Wan In Lee. Preparation of size-controlled TiO_2 nanoparticles and derivation of optically transparent photocatalytic films. *Chemistry of Materials*, 15(17):3326–3331, 2003.

[33] R.Lee Penn and Jillian F Banfield. Morphology development and crystal growth in nanocrystalline aggregates under hydrothermal conditions: insights from titania. *Geochimica et Cosmochimica Acta*, 63(10):1549 – 1557, 1999.

[34] Barbara Horvat, Aleksander Rečnik, and Goran Dražić. The growth of anatase bipyramidal crystals during hydrothermal synthesis. *Journal of Crystal Growth*, 347(1):19 – 24, 2012.

[35] Hidehiro Kamiya Motoyki Iijima, Murino Kobayakawa. Tuning the stability of TiO_2 nanoparticles in various solvents by mixed silane alkoxides. *Journal of Colloid and Interface Science*, 337:61–65, 2009.

[36] M. Sabzi, S.M. Mirabedini, J. Zohuriaan-Mehr, and M. Atai. Surface modification of TiO_2 nano-particles with silane coupling agent and investigation of its effect on the properties of polyurethane composite coating. *Progress in Organic Coatings*, 65(2):222 – 228, 2009.

[37] Emi Ukaji, Takeshi Furusawa, Masahide Sato, and Noboru Suzuki. The effect of surface modification with silane coupling agent on suppressing the photo-catalytic activity of fine TiO_2 particles as inorganic UV filter. *Applied Surface Science*, 254(2):563 – 569, 2007.

[38] Dorota Koziej, Fabian Fischer, Niklaus Kränzlin, Walter R. Caseri, and Markus Niederberger. Nonaqueous TiO_2 nanoparticle synthesis: a versatile basis for the fabrication of self-supporting, transparent, and uv-absorbing composite films. *ACS Applied Materials & Interfaces*, 1(5):1097–1104, 2009. PMID: 20355897.

[39] Hongxia Zhao and Robert K.Y. Li. A study on the photo-degradation of zinc oxide (ZnO) filled polypropylene nanocomposites. *Polymer*, 47(9):3207 – 3217, 2006.

[40] Yuan-Qing Li, Shao-Yun Fu, and Yiu-Wing Mai. Preparation and characterization of transparent ZnO/epoxy nanocomposites with high-UV shielding efficiency. *Polymer*, 47(6):2127 – 2132, 2006.

[41] Yuanrong Cheng, Changli Lu, Zhe Lin, Yifei Liu, Cheng Guan, Hao Lu, and Bai Yang. Preparation and properties of transparent bulk polymer nanocomposites with high nanophase contents. *J. Mater. Chem.*, 18:4062–4068, 2008.

[42] Carlos A. García-González, Julio Fraile, Ana López-Periago, and Concepción Domingo. Preparation of silane-coated TiO_2 nanoparticles in supercritical CO_2. *Journal of Colloid and Interface Science*, 338(2):491–499, 2009.

[43] Bruker Corporation. *PeakForce QNM user guide, 004-1036-000.*

[44] Perla B. Balbuena and Keith E. Gubbins. Theoretical interpretation of adsorption behavior of simple fluids in slit pores. *Langmuir*, 9(7):1801–1814, 1993.

[45] M.M. Viana, V.F. Soares, and N.D.S. Mohallem. Synthesis and characterization of TiO_2 nanoparticles. *Ceramics International*, 36(7):2047 – 2053, 2010.

[46] A. Dalod. *Unpublished data.* NTNU, Norway, 2016.

Appendix A

Rietvield refinement for 10:1-basic and 10:1-acidic

Rietvield refinement done for the samples 10:1-acidic and 10:1-basic (sample showing the largest difference in morphology). Bars in both figures indicates diffraction peaks for anatase from ICDD card #00-021-1272. 10:1-basic shows a much larger difference between the observed and calculated values for the (004) peak than 10:1-acidic, indicating anisotropic crystallite sizes.

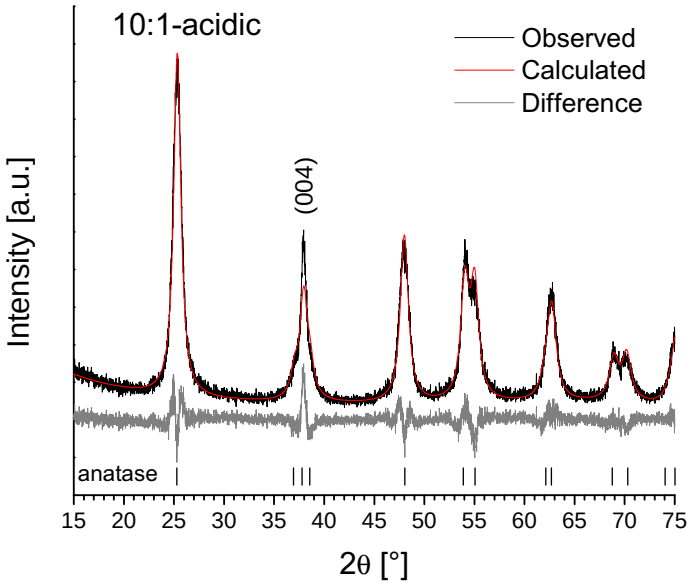

Figure A.1: Rietvield refinement for 10:1-acidic.

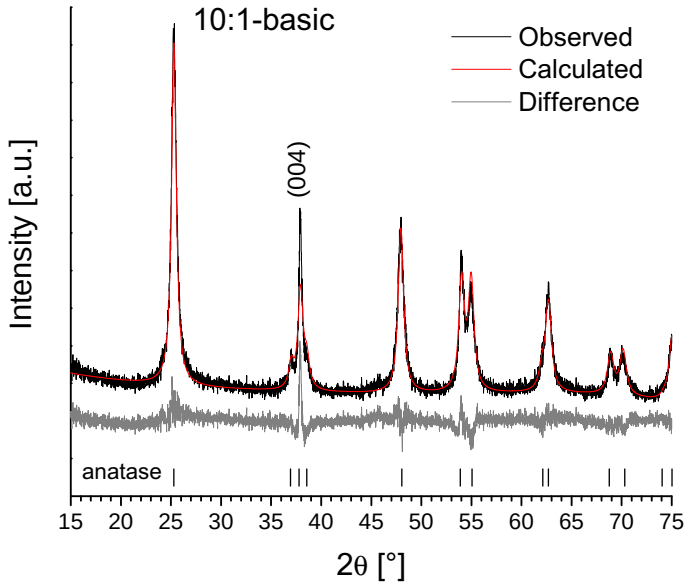

Figure A.2: Rietvield refinement for 10:1-basic.

Appendix B

FTIR spectra

FTIR spectra for the samples prepared as a part of the authors specialization project is presented here. Samples prepared with 10:1 molar ratio is in Figure B.1, and 15:1 molar ratio is in Figure B.2. For both plots the samples are labeled as follows, a) Ti-ref, b) A-15min, c) A-30min, d) A-60min, e) A-120min.

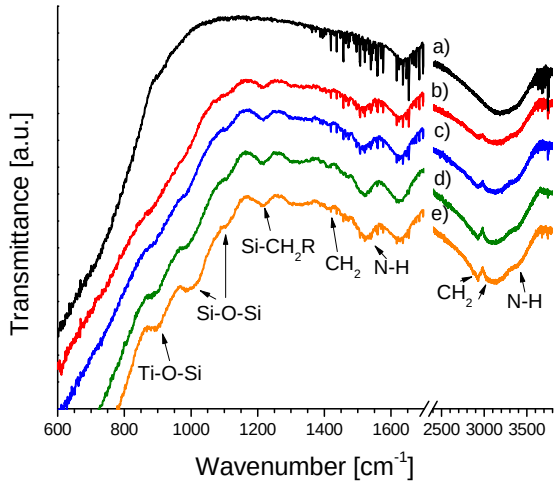

Figure B.1: FTIR spectra for samples prepared with 10:1 molar ratio for the specialization project of the author.

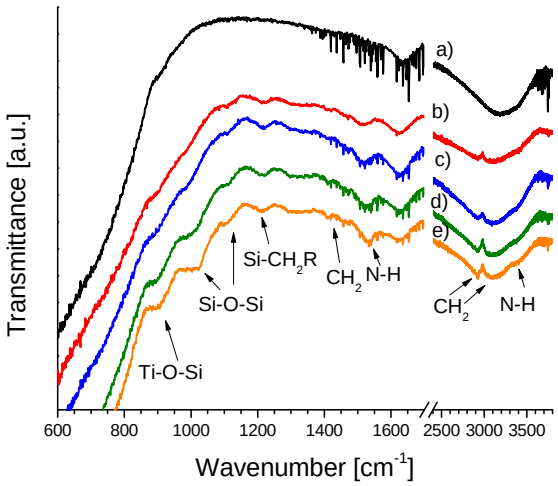

Figure B.2: FTIR spectra for samples prepared with 15:1 molar ratio for the specialization project of the author.